Doctoral Dissertation

Si Surface Passivation by Atmospheric-Pressure Plasma Oxidation

Zeteng Zhuo

January 2014

Graduate School of Engineering,

Osaka University

Table of Contents

Chapter 1

Introduction

1.1 General introduction

The world energy demand is growing rapidly: the total energy consumption on earth is expected to increase by 0.7 – 1.4% per year in the period ranging from 2008 to 2035, depending on the chosen energy scenario [1,2]. This increasing demand is mainly caused by (i) a fast growing world population (approximately 9 billion people in 2050 versus 6 billion in 2000) and (ii) fast economic growth in countries such as China and India. Nowadays, the world energy market is dominated by fossil fuels, i.e. oil (40%), coal (33%) and natural gas (27%). In 2008, fossil fuels accounted for 81% of the total world energy consumption [1]. Due to limited resources and environmental impact, this consumption cannot be sustained in the long term, and new sources of energy generation have to be explored. Moreover, due to the fossil fuel consumption which caused the global warming, humankind is looking for alternative way of producing power such as new energy materials including solar energy, which can lead to minimal CO_2 emission.

Solar constant is defined as the average amount of energy from the sunlight incident on a plane perpendicular to the direction of the photons outside the earth's atmosphere, and is equal to 1366 W/m^2 [3]. This leads to a total irradiation on the earth's surface in the order of 10^{24} J, which is roughly 2000 times the actual world energy consumption. This clearly demonstrates that solar energy has, at least in theory, the potential to supply the global energy demand. In general, solar energy are highly promising

candidates.

Solar energy conversion can generally be divided into two different technologies: solar thermal and photovoltaics (PV). In solar thermal, energy from sunlight is converted into heat for domestic use or for conversion to electricity in large size concentrated solar power plants, whereas in PV, energy from sunlight is directly converted into DC electricity. Now, the dominating photovoltaic components is still the "bulk" or wafer-based crystalline silicon. Over the past few years, the market share of PV in global energy has increased substantially. In 2010, an estimated record solar cell production of 23.9 GW was realized; a 123% increase over 2009 [4-6]. The world PV market is expected to increase further by 33% on average per year until at least 2014.

1.2 Principles of photovoltaic solar energy

Solar cell is a device that converts the energy of light to the electricity. In most cases, semiconductor is used for solar cell material. The energy conversion consists of absorption of photon to generate electron-hole pairs in a semiconductor and charge carrier separation. A p-n junction is used for charge carrier separation in most cases.

In solar cells, sunlight is directly converted into DC electricity, using the photovoltaic effect which was first discovered by Becquerel in 1839 [7]. The basic steps needed for photovoltaic energy conversion are explained as follows: when photons are incident on a semiconductor, they can be absorbed in the bulk material depending on the photon energy and the band gap of the material, resulting in the excitation of valence electrons into the conduction band. A high mobility facilitates the charge transport within the conduction band of the semiconductor material. The energy difference

between valence and conduction band is referred to as the band gap, for which several operational definitions are in use. For semiconductors, typical band gap values are located within the visible or near infrared part of the solar spectrum, which is most suitable to convert sunlight into electricity [8]. In the presence of an electric field typically related with a p-n junction, charge separation can take place and photogenerated charge carriers can be extracted from the device. This way, sun light is converted into DC electricity. Semiconductor materials that are most commonly used for solar cell fabrication are Si, Ge, GaAs, CdTe, CdSe, copper indium (gallium) selenide (CI(G)S), as well as several organic materials.

Silicon is the most developed and well-understood semiconductor material in the world, benefiting from long duration of research and development in the academic society and the integrated circuit industry. Techniques to control the properties of semiconductor material are well established. Silicon has proven field stability, and it is the most abundant semiconductor on the earth. In this thesis, the research content is focused on silicon solar cells.

1.3 Crystalline silicon solar cells and surface passivation

1.3.1 Developmental trend of crystalline silicon solar cells

The PV market is still dominated by crystalline silicon (c-Si) solar cells, especially due to the wide abundance of Si, its low cost and non-toxicity. In 2010, the market share of c-Si based solar cells was equal to 87% [5]. Crystalline silicon based PV has this impressive market share as it combines state-of-the-art production techniques with high (> 15%) module efficiencies, off-the-shelf manufacturing equipment. However, current trend in the silicon photovoltaic industry is the cost-driven reduction of the

solar cell thickness. The developmental trend of Si photovoltaics moves toward much thinner cells than 150 μm. An important aspect in reducing the silicon solar cell thickness is that the recombination of minority carriers at surfaces and interfaces plays a larger role, affecting the cell performance. Figure 1-1 shows the surface and bulk recombination losses occur via defect levels within the band gap. Therefore the passivation of the surface is one of the key importance for the efficiency of thin silicon solar cells.

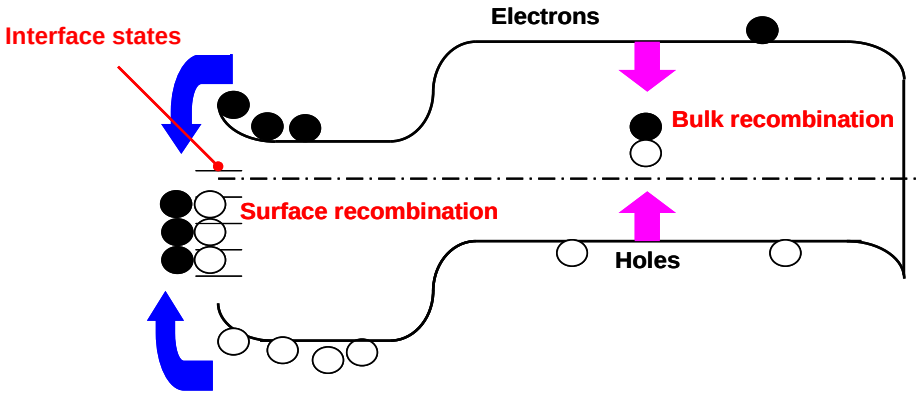

Fig.1-1 Surface and bulk recombination of generated charge carriers.

Obviously, with reducing the cell thickness, technology for improving the energy conversion efficiency of Si thin solar cells is indispensable. Therefore, the development of technology for improving conversion efficiency, for example, effective surface passivation process is becoming increasingly important for Si based thin solar cells and the reduction of surface recombination loss can provides a potential of remarkable improvement in solar cell energy conversion efficiencies.

1.3.2 Surface recombination and passivation

Due to the non-saturated bonds, a large number of defects within the

bandgap exist at the material surface. In the surface recombination process, excited electrons in the conduction band recombine with holes in the valence band via defect levels at the surface, called surface states. In order to decrease surface recombination losses at c-Si surfaces at tolerable levels, the c-Si surfaces must be well electrically passivated. High quality surface passivation film can reduce recombination losses at the c-Si surface and reflection losses. Generally, surface passivation is ascribed to two different phenomena, namely *chemical passivation* and *field effect passivation*. The former is caused by a reduction of defect states at the c-Si surface, and the latter by repulsion of minority charge carriers from the interface by fixed charges as illustrated in Fig.1-2.

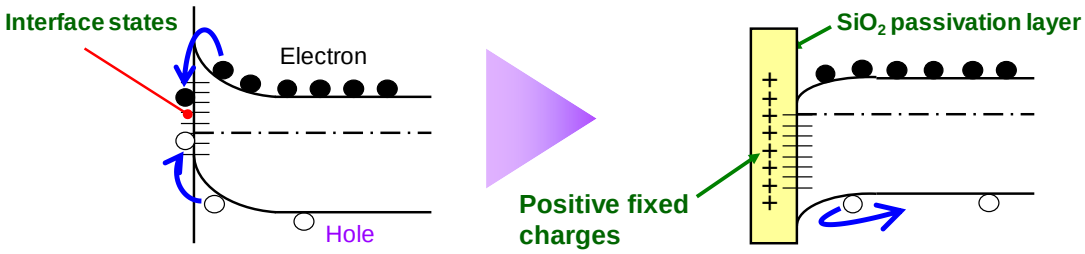

Fig.1-2 Repulsion of minority carriers from the interface by the positive fixed charges in SiO_2 passivating layer.

Besides surface recombination, bulk recombination should also be minimized. Bulk recombination is predominantly governed by three different recombination mechanisms, i.e., Shockley-Read-Hall (SRH) recombination [9,10], auger recombination [11] and radiative recombination [12]. SRH recombination accounts for the recombination through defect states within the band gap and is mostly dependent on the quality of the used c-Si substrates. Radiative recombination is basically the

inverse process of generation: an electron in the conduction band and a hole in the valence band recombine, thereby releasing the excess energy as a photon. In c-Si, radiative recombination rates are low due to the indirect band gap of the material, which requires the coupling with a phonon for momentum conservation. In auger recombination, an electron and a hole recombine, transferring the excess energy to a third carrier (either an electron in the conduction band or a hole in the valence band) to be excited into energy states deeper in the respective band. This excess energy is subsequently released to the crystal lattice in the form of heat.

In the rest of this thesis, only surface recombination will be further taken into account. The focus of this research is on the field-effect passivation of Si surface due to electrical charges in the passivating film.

1.3.3 Overview of various materials for surface passivation of crystalline silicon

Surface passivation is a key requirement for optimizing the performance of several types of c-Si based solar cells. To obtain high open circuit voltages in such devices, excellent surface passivation is required [13]. Various materials have been studied for surface passivation, such as thermally grown SiO_2 [14], silicon nitride (SiN_x) [15,16], aluminum oxide (Al_2O_3) [17,18], amorphous silicon sub-oxides (a-SiO_x) [19,20], amorphous silicon carbide (a-SiC_x) [21,22] and hydrogenated amorphous silicon (a-Si:H) [23–26]. Furthermore, excellent results on combined layer stacks of these materials have been reported, such as the stacks consisting of a-Si:H/SiN_x [27,28] and thermal SiO_2/SiN_x [29]. All these materials have their particular advantages, drawbacks and possible applications.

Thermally grown (T > 1000°C) SiO_2 has traditionally been the common

method to obtain high quality c-Si surface passivation [14]. Kerr *et al.* have demonstrated very low surface recombination velocities (SRV < 0.46 cm/s) with this material on high resistivity (ρ = 90 Ωcm) n-type c-Si float-zone (FZ) wafers [14]. In the regime of low processing temperatures (T < 200°C), a-Si:H is the best and most widely used material. Using a-Si:H layers with thicknesses of approximately 50 nm, extremely low surface recombination velocities (SRV ~ 1 – 3 cm/s) have been obtained by various deposition techniques [23]. Currently, the most commonly used surface passivation scheme in large-scale c-Si PV production is a-SiN_x deposited by plasma-enhanced chemical vapor deposition (PECVD) due to its combined passivation and antireflection properties. The positive fixed charges in SiN_x layers cause field effect passivation on n-type c-Si, as in this case the minority charge carriers (holes) are repelled from the c-Si surface. In 1996, Lauinger *et al.* have already reported on surface recombination velocities of 4 cm/s and 20 cm/s on 1.5 Ωcm and 0.7 Ωcm p-type (100) oriented double sided polished c-Si wafers passivated on both sides by SiN_x films deposited by remote PECVD [30]. In 2010, Koyama *et al.* have reported on passivating layer stacks consisting of intrinsic a-Si:H (10 nm thickness) and a-SiN_x:H (100 nm thickness), both deposited by hot-wire chemical vapor deposition (HWCVD), showing surface recombination velocities below 9.0 cm/s on (100) oriented FZ p-type c-Si wafers (ρ ~ 2.0 Ωcm) and below 1.5 cm/s on (100) oriented FZ n-type c-Si wafers (ρ ~ 2.5 Ωcm) [28]. Such outstanding results on n-type wafers are due to the combination of chemical passivation by the intrinsic a-Si:H and the field effect passivation of the a-SiN_x:H overlayer.

Al_2O_3 has become increasingly popular as a surface passivating material, especially for p-type c-Si due to its high negative fixed charge density [18].

Al_2O_3 films can be deposited by various deposition techniques, i.e. atomic layer deposition (ALD) [17,18], PECVD [31] and radio frequency (RF) magnetron sputtering [32]. Al_2O_3 films can yield surface recombination velocities below 2 cm/s for layers fabricated at a high deposition rate of 1.2 nm/s [33]. Annealing at T ~ 350°C is a crucial step to obtain the lowest surface recombination velocities for this material [18,33]. Recently, it has also been reported that SiO_xN_y passivating film with a high positive fixed charge density in the range of 10^{11-12} cm^{-2} is effective for minimizing the recombination losses at the interfaces. Several methods have been applied to grow SiO_xN_y films, such as the direct thermal oxyntridation of Si in NO or N_2O ambient [34,35] and annealing of SiO_2 in nitrogen containing ambient [36,37]. These methods, however, need high temperature process steps (T > 900°C).

Other than the above methods for preparing the passivating layer, this thesis presents an experimental study on a new process to form high-quality passivating films (SiO_2, SiO_xN_y and AlO_x) using atmospheric-pressure (AP) plasma generated by a 150MHz very high frequency (VHF) electric field.

1.4 The aim of this research

The objective of this research is to develop a new preparation process at low temperatures (T ≤ 400°C) for forming high-quality passivating films (SiO_2, SiO_xN_y and AlO_x) with low interface state density (D_{it}) and high fixed charge density (Q_f) by using AP plasma generated by a 150MHz VHF electric field.

SiO_2 is the standard surface passivation materials. SiO_2 has inherent advantages and drawbacks: using high-temperature thermal oxidation processes (T > 900°C), SiO_2 layers with low D_{it} (of the order of 10^{10}

$cm^{-2}eV^{-1}$) have been obtained on moderately-doped Si substrates. However, the high-temperature process may deteriorate the bulk Si quality and reduce the bulk carrier lifetime, especially for the lower quality Si materials [e.g., multi-crystalline Si or Czochralski Si (CZ-Si)] than FZ-Si. SiO_2 films with D_{it} of the order of 10^{10} $cm^{-2}eV^{-1}$ have been obtained by PECVD at 200 – 400°C followed by a forming gas anneal. However, the properties of SiO_2 films prepared by PECVD are affected by impurities (H, N, H_2O, Si-OH groups), and are characterized by a higher porosity compared to thermally-grown SiO_2 films at higher temperatures.

The high temperature process (T > 900°C) has been applied to grow SiO_xN_y films suffer a much higher thermal budget and dopant diffusion problem. In order to reduce the thermal budget in the fabrication of SiO_xN_y films, low-temperature process steps (T ≤ 400°C) is an alternative. For example, chemical-vapor deposition (CVD) was applied. However, CVD method needs toxic precursor source [38-40], and it is also noted that in the films prepared by the low-temperature PECVD, the concentration of hydrogen atoms in the form of Si–OH and Si–H bonds is high, which is responsible for deteriorating their dielectric properties.

The most common deposition technique for forming Al_2O_3 layer was ALD method [17,18]. However, the ALD technique cycles reactant gas insertions and purges in order to achieve a precisely controlled deposition, atomic layer by atomic layer. Therefore typically low deposition rates (< 2 nm/min) of ALD limit its application in a commercial production line [41,42].

Other than the above methods for preparing the passivating layer, AP VHF plasma oxidation or oxidation-nitridation (T ≤ 400°C) can be used as an alternative approach to prepare passivating films (SiO_2, SiO_xN_y and

AlO_x). The AP plasma generated by a 150MHz VHF electric field is a stable glow and a high-density plasma for increasing the reactive rate. In AP VHF plasma process, the kinetic energy of charged species is so low that ion damages induced in the substrate, interface or growing film can be minimized. Additionally, the low-temperature AP VHF plasma oxidation or oxidation-nitridation processes have a potential to reduce fabrication costs of thin films. This method also has some advantages, such as the small plasma gap ($\leq$ 1mm) between the electrode and sample which may promote efficient chemical reactions, and the usage of only O_2 and rare gas as source gases without being accompanied by chemical residue etc. Moreover, the AP plasma oxidation process is compatible for the open air process, which is very attractive for photovoltaic industry as a high-throughput process for preparing functional films. Therefore, it can be expected that the AP plasma oxidation method is a new and high efficient way to the formation of a high quality passivating layer.

In this thesis, the AP VHF plasma oxidation and oxidation-nitridation processes are studied. The correlation of AP VHF plasma process parameters and the resulting functional layer properties is quite complex. We think that the film growth and the resulting material properties are critically dependent on the AP VHF plasma characteristics. Therefore, a good comprehension of the AP VHF plasma oxidation process parameters can give good directions for more improvements to form high-quality passivating film.

1.5 Thesis outline

This thesis is structured as follows:

Chapter 1 introduces the background of this work. Principles of

photovoltaic solar energy and the c-Si solar cells are especially focused on. Finally, the fundamentals of surface passivation and overview of various materials for surface passivation of c-Si are described.

In chapter 2, overview of plasma oxidation technology and its application for semiconductor devices are given. The basic properties of AP VHF plasma are also described.

Chapter 3 describes the AP plasma generated by a 150 MHz VHF electric field which used as oxidation of Si wafer at 400°C for forming SiO_2 films and investigation of material-qualities of SiO_2 films. Surface passivation quality of SiO_2 passivating film is also investigated.

Chapter 4 describes formation of SiO_xN_y passivating films on Si substrates at 400°C by AP plasma oxidation-nitridation process using O_2 and N_2 as gaseous precursors diluted in He. The influence of AP VHF plasma oxidation-nitridation process parameters on the interface electrical properties and chemical elements of the nitrided oxides are studied.

In chapter 5 the formation and characterization of AlO_x film by AP VHF plasma oxidation process at 400°C was introduced. Especially, the Q_f and D_{it} at AlO_x/Si interface using SiO_2 interlayer are investigated.

In chapter 6, a summary of the thesis is given.

References

[1] International Energy Agency, World Energy Outlook **2010** (2010).

[2] U.S. Energy Information Administration, International Energy Outlook **2010** (2010).

[3] S. Darula, L. Kittler, and C.A. Gueymard, Solar Energy **79** (2005) 559.

[4] S. Metha, PV News **29-10** (2010) 3.

[5] S. Metha, PV News **30-5** (2011) 3.

[6] European Commission Joint Research Centre Institute for Energy, PV Status

Report **2010** (2010).

[7] A.E. Becquerel, Comptes Rendus de l'Academie des Sciences **9** (1839) 145.

[8] W. Shockley, and H.J. Queisser, J. Appl. Phys. **32** (1961) 510.

[9] W. Shockley, and W.T. Read Jr., Phys. Rev. **87** (1952) 835.

[10] R.N. Hall, Phys. Rev. **87** (1952) 387.

[11] M.J. Kerr, and A. Cuevas, J. Appl. Phys. **91** (2002) 2473.

[12] W. Michaelis, and M.H. Pilkuhn, Phys. Stat. Sol. A **36** (1969) 311

[13] Y. Tsunomura, Y. Yoshimine, M.Taguchi, T. Baba, T. Kinoshita, H. Kanno, H. Sakata, E. Maruyama, and M. Tanaka, Sol. Energy Mater. Sol. Cells **93** (2009) 670.

[14] M. J. Kerr, and A. Cuevas, Semicond. Sci. Technol. **17** (2002) 35.

[15] V. Verlaan, C.H.M. van der Werf, Z.S. Houweling, H.F.W. Dekkers, I.G. Romijn, A.W. Weeber, H.D. Goldbach, and R.E.I. Schropp, Prog. Photovolt: Res. Appl. **15** (2007) 563.

[16] M.J. Kerr, J. Schmidt, A. Cuevas, and J.H. Bultman, J. Appl. Phys. **89** (2001) 3821.

[17] B. Hoex, J. Schmidt, P. Pohl, M.C.M. van de Sanden, and W.M.M. Kessels, J. Appl. Phys. **104** (2008) 044903.

[18] F. Werner, B. Veith, V. Tiba, P. Poodt, F. Roozeboom, R. Brendel, and J. Schmidt, Appl. Phys. Lett. **97** (2010) 162103.

[19] H. Fujiwara, T. Kaneko, and M. Kondo, Appl. Phys. Lett. **91** (2007) 133508.

[20] T. Mueller, S. Schwertheim, M. Scherff, and W.R. Fahrner, Appl. Phys. Lett. **92** (2008) 033504.

[21] I. Martín, M. Vetter, A. Orpella, C. Voz, J. Puigdollers, and R. Alcubilla, Appl. Phys. Lett. **81** (2002) 4461.

[22] C. Ehling, J.H. Werner, and M.B. Schubert, Phys. Stat. Sol. C **7** (2010) 1016.

[23] J.W.A. Schüttauf, C.H.M. van der Werf, I.M. Kielen, W.G.J.H.M.van Sark, J.K. Rath, and R.E.I. Schropp, Appl. Phys. Lett. **98** (2011) 153514.

[24] S. De Wolf, S. Olibet, and C. Ballif, Appl. Phys. Lett. **93** (2008) 032101.

[25] J. Damon-Lacoste, L. Fesquet, S. Olibet, and C. Ballif, Thin Solid Films **517** (2009) 6401.

[26] T.F. Schulze, H.N. Beushausen, C. Leendertz, A. Dobrich, B. Rech, and L. Korte,

Appl. Phys. Lett. **96** (2010) 252102.

[27] S. Gatz, H. Plagwitz, P.P. Altermatt, B. Terheiden, and R. Brendel, Appl. Phys. Lett. **93** (2008) 173502.

[28] K. Koyama, K. Ohdaira, and H. Matsumura, Appl. Phys. Lett. **97** (2010) 082108.

[29] Y. Larionova, V. Mertens, N.-P. Harder, and R. Brendel, Appl. Phys. Lett. **96** (2010) 032105.

[30] T. Lauinger, J. Schmidt, A.G. Aberle, and R. Hezel, Appl. Phys. Lett. **68** (1996) 1232.

[31] P. Saint-Cast, D. Kania, M. Hofmann, J. Benick, J. Rentsch, and R. Preu, Appl. Phys. Lett. **95** (2009) 151502.

[32] T.-T. Li, and A. Cuevas, Phys. Stat. Sol. RRL **3** (2009) 160.

[33] P. Poodt, A. Lankhorst, F. Roozeboom, K. Spee, D. Maas, and A. Vermeer, Adv. Mater. **22** (2010) 3564.

[34] E. P. Gusev, H. C. Lu, T. Gustafsson, E. Garfunkel, M. L. Green, and D. Brasen, J. Appl. Phys. **82** (1997) 1997.

[35] H.C. Lu, E. Gusev, N. Yasuda, M. Green, G. Alers, E. Garfunkel, and T. Gustafsson, Appl. Surf. Sci. **166** (2000) 465.

[36] T. Hori, T. Yasui, and S. Akamatsu, IEEE Trans. Electron Dev. **39** (1992) 134–147.

[37] Z-Q. Yao, H.B. Harrison, S. Dimitrijev, and Y. Yeow, IEEE Electron Dev. Lett. **16** (1995) 345–347.

[38] Zhenrui Yu, Mariano Aceves, Jesus Carrillo, and Rosa López-Estopier, Thin Solid Films **515** (2006) 2366.

[39] D. Criado, A. Zuniga, and I. Pereyra, J Non-Crystalline Solids **354** (2008) 2809.

[40] K.F. Albertin, and I. Pereyra, J Non-Crystalline Solids **354** (2008) 2646.

[41] T. T. Li, and A. Cuevas, Phys. Status Solidi RRL **3** (2009) 160.

[42] P. Saint-Cast, D. Kania, M. Hofmann, J. Benick, J. Rentsch, and R. Preu, Appl. Phys. Lett. **95** (2009) 151502.

Chapter 2

Overview of plasma oxidation technology and its application for semiconductor devices

2.1 Overview of plasma oxidation technology

2.1.1 Kinetics of SiO_2 growth in oxygen plasma

Silicon dioxide (SiO_2) is one of the most important materials in semiconductor device manufacturing, having played an important role in the development of semiconductor planar process. The formation of SiO_2 on a Si surface is commonly accomplished by a process called thermal oxidation (usually between 700~1300°C). The thermal oxidation is known to be the best way for obtaining high quality SiO_2 films with good chemical and electrical properties. These oxidation reactions occur at the Si-SiO_2 interface, i.e., Si at the interface is consumed when oxidation reaction takes place. Furthermore, the high-temperature process at around 1000°C may deteriorate the bulk Si quality and reduce the bulk carrier lifetime, especially for the lower quality Si materials [e.g., multi-crystalline Si or CZ-Si than FZ-Si [1]. Thermal oxidation cannot avoid the defect formation associated with the volume expansion of SiO_2 compared to Si and the interfacial stress arising from the different thermal expansion coefficient of SiO_2 from that of Si. Thus, ceaseless efforts of downsizing metal–oxide–semiconductor (MOS) devices require the formation of high-quality SiO_2 layer at temperatures as low as 150 – 400°C by oxidation of Si in plasma.

In this chapter, some experimental systems for plasma oxidation which have been reported in the literature are reviewed and compared. The

reported kinetics of oxide layers grown by plasma oxidation is also introduced, together with the material-properties of the grown oxide layers. Plasma oxidation is a very prospective technology, because it offers not only a rapid growth process of a SiO_2 layer of high electrical quality, but also a low-temperature process far below those required for thermal oxidation. In the low-temperature plasma oxidation process, dopant redistribution is minimized during oxide growth and the high-temperature induced defects (e.g. stacking faults) in the Si wafer are also reduced. There have been numerous studies of plasma oxidation, including those using electron cyclotron resonance (ECR) plasma [2], helicon plasma [3] and downstream microwave plasma [4]. Some experimental systems use a DC glow discharge to sustain the plasma [5,6]. The plasmas excited in other experimental systems are obtained by capacitively coupled electrodes [7,8]. Both of these methods suffer from a relatively low oxide growth rate compared with the method using an inductively coupled plasma. When a DC bias is superimposed across the discharge, the method is called as plasma anodization [9-11].

The reported kinetics of plasma oxidation differ widely depending upon the kinds of oxidant species generated in the different oxidative conditions. And various ideas in the published literature have been proposed to interpret the mechanism of oxide growth in the different oxidant species. In case of the plasma oxidation, the SiO_2 surface contacts the plasma with the influx of several kinds of neutral (O_2 molecules, O radicals) and charged species (electrons, O^+, O_2^+, O^-). The question is what species play the key role for the oxygen transport to the SiO_2–Si interface.

Some authors believe that plasma oxidation is dominated by oxygen atoms (O radicals) in the growth process of SiO_2 upon Si in oxygen plasma

[12]. Recently, it has been also founded that the highly reactive nature of the O radical is believed to be responsible for the efficient oxidation process at such a low temperature [13]. About this hypothesis of plasma oxidation, the most promising result was reported by Ohmi's group [12]. High-quality SiO_2 thin films were formed at 400°C in un-magnetized microwave plasma in various kinds of inert gas containing a few percentage of O_2 (less than 3%), among which krypton (Kr) gas provided the highest oxidation rate and the film quality comparable to thermally grown oxide [12]. This result was tentatively explained in terms of radical oxidation where the key species for oxidation is regarded to be O radicals produced in rare gas microwave discharges, most efficiently by metastable Kr atoms in discharges. However, the model of radical oxidation where the O radicals primarily oxidize the silicon is excluded because there was no correlation between the O radical density and the oxidation rate.

It has also been reported that negative oxygen species is responsible for the oxidation process [14,15]. Recently, Hasegawa *et al.* have shown that the oxidation rate is proportional to the square root of electron density but hardly correlates with the measured O radical density in microwave plasma of argon gas containing a few percent of O_2 [16,17]. Moreover, secondary ion mass spectrometry (SIMS) depth analysis of SiO_2 layer with ^{18}O as an isotope tracer suggests that predominant mobile species in the oxide layer is not neutral oxygen atom but oxygen negative ion (possibly O^{2-}) and that the plasma oxidation mechanism can be explained based on the Jorgensen-Mott model [18,19] which assumes negative oxygen ions as transporting species.

Other ideas have also been supposed to explain the kinetics and growth mechanism of oxide layers in oxygen plasma. For example, it has been

reported that that field-assisted cation (Si^+) and O^- anion diffusion through the growing film is the growth mechanism of oxide layers. [9,20]. However, Perriere *et al.* showed that for cations the transport number was zero, indicating only the O^- anions was responsible for the oxide layer formation [21]. Kimura *et al.* also showed the same conclusion by using SIMS and ^{18}O as a tracer in their experiment [2]. Some workers have further suggested that the singly charged oxygen ion, such as O^-, is the species responsible for the growth mechanism of oxide layers in the low-temperature oxidation [15,22]. The independence of oxide growth rate upon the orientation of the Si surface is the same observation for all the plasma oxidation [23]. This is in contrast to the thermal oxidation in which the growth rate of oxide film is strongly dependent on the orientation of the Si surface.

Finally, various experimental systems for plasma oxidation of Si wafers are summarized in Table 2-1.

Table 2-1 Examples of low-temperature plasma oxidations for Si.

Plasma gas	Freq. (MHz)	O_2 (%)	Pressure (Pa)	Power (W)	Temp. (°C)	Sample Size (mm)	Oxidation rate (nm/min)	DC bias (V)	D_{it} ($cm^{-2}eV^{-1}$)	Q_f (cm^{-2})	Refractive index	Author
Ar	2450	1.4	150	1000 – 3000	400	ϕ200	1.0 – 3.0	0	–	–	–	**Hasegawa** *et al.* [16, 17]
O_2	2450 ECR	100	0.13	320 – 375	260 - 390	ϕ100	1.8 – 3.4	+5 MV/cm	2.0×10^{11}	6.0×10^{11}	1.465	**Martinet** *et al.* [24]
H_2	2450	30–100	13.3	500 - 2000	150 - 320	ϕ150-300	5.0~6.0	0	6.0×10^{10}	–	–	**Lerch** *et al.* [25]
Kr	2450	3 or 100	80	1200	300	ϕ200	~2.5	0	4.0×10^{10}	–	–	**Goto** *et al.* [26]
Ar	2450 ECR	~28	10^{-2} – 10^{-1}	500	room temperature	ϕ150	~6.0	–	3.0×10^{10}	–	–	**Saito** *et al.* [27]

2.1.2 Physical properties of SiO_2 films grown by plasma oxidation

The material properties, density and refractive index of the oxide films obtained by the plasma oxidation of Si wafers were almost indistinguishable from thermally grown oxides. Ho and Sugano has used infrared absorption spectroscopy to show that the absorption peaks of plasma grown oxides appear at the same positions as those for high-temperature thermal oxides [20]. However, Nelson *et al.* found some detailed differences at the interface in thermal, rapid thermal and plasma oxides by X-ray photoelectron spectroscopy (XPS) [28]. Furthermore, the electron conduction mechanism in plasma grown oxides has been found to be the same as that in thermally grown oxides, i.e. by Fowler-Nordheim tunneling of electrons into the oxide conduction band. The fixed oxide charges may be obtained in the order of 10^{11} cm^{-2} for plasma-grown oxides. Detailed examination of the interface of plasma-grown oxide revealed that interface trap density (D_{it}) (in the order of 10^{10} $cm^{-2}eV^{-1}$) was as low as those obtained by high-temperature thermally grown oxide. Some authors have shown that the plasma-grown oxides have a mean electrical breakdown strength in excess of 10 MV cm^{-1} [29].

2.1.3 Applications for semiconductor devices

High-temperature thermal oxidation of Si is commonly used to form high quality SiO_2 in Si integrated circuit technology. The thermally grown SiO_2 is used for the gate oxide and can also be used for device isolation (field oxide). However, the high temperature process results in several drawbacks: dopant atoms can redistribute and the impurity concentrations of each layer can vary; defects (oxidation induced stacking faults) are often found. Low-temperature plasma oxidation is a promising alternative for the

formation of functional thin films, such as the gate dielectrisc in polycrystalline Si thin-film transistors (TFT) on glass substrates for liquid crystal displays [30]. It is impossible to use high-temperature thermally grown SiO_2 in this application since the softening point of the glass substrates inhibits the use of temperatures above 600°C. The plasma grown oxides with excellent electrical properties have also allowed to use as MOS gates for ultra-large-scale integrated (ULSI) circuits [31].

Recently, many researches are to develop a plasma oxidation process of high-quality SiO_2 passivation film applicable for surface passivation of Si solar cells. As surface passivation films, the required properties for SiO_2 films are dense structure and low D_{it} comparable to those of high-temperature thermal oxides. Moreover, in contrast to the application for gate oxides in ULSIs or TFTs, a high positive fixed oxide charge density (Q_f) is desirable for field-effect passivation of n-type Si surfaces.

2.2 AP VHF plasma oxidation technology

2.2.1 Experimental apparatus

AP VHF plasma is a new technique that has attracted much attention compared to the standard RF plasma. The excitation frequency of the present AP plasma is 150 MHz, enabling higher growth rates while maintaining the material quality. Furthermore, because of the lower ion energies, the ion bombardment onto the film surface is reduced. Figure 2-1 (a) and (b) shows the photograph and schematic illustration of AP VHF plasma oxidation apparatus, respectively. Substrate was transferred to the main body of the reactor with a base pressure less than 10^{-6} Torr, and then the reactor was filled with a process gas mixture of 0.5 - 5%O_2/ He at 760 Torr. During oxidation, AP plasma was excited with a moderately large

VHF power of about 1000 W. By virtue of these noble characteristics of the system, passivating films can be fabricated.

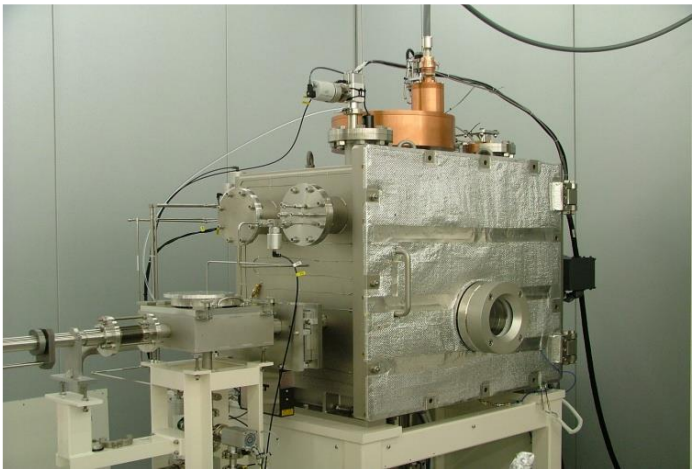

Fig.2-1 (a) Photograph of AP plasma oxidation apparatus.

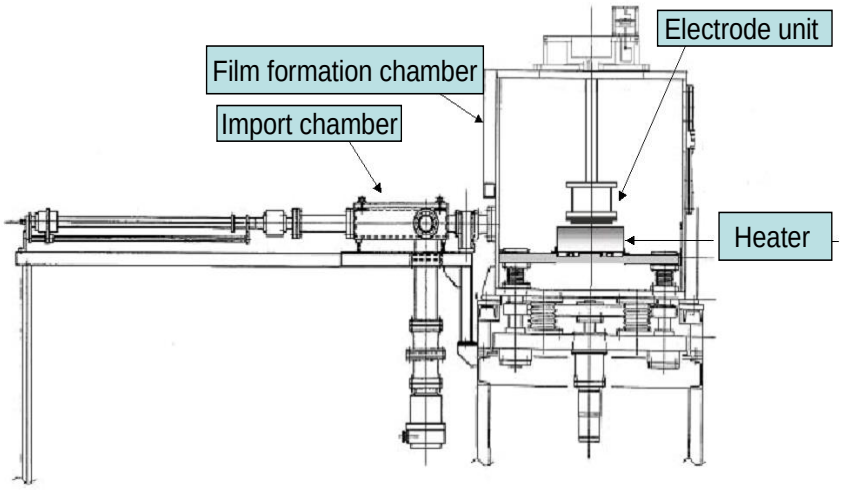

Fig.2-1 (b) Schematic diagram of the AP plasma oxidation apparatus.

2.2.2 Characteristics of AP VHF plasma

The low-pressure plasma oxidation technique has mainly been adopted in film fabrication processes. However, several problems have arisen in the practical application of conventional low-pressure plasma oxidation technique, such as low oxidation rate and high ion energy. Effective methods to reduce ion energies while maintaining high deposition rates are the use of VHF excitation of the plasma [32,33]. In this research, AP plasma generated by a 150MHz VHF electric field is applied for the oxidation process. A few part of O_2 gas is diluted by a large amount of inert gas such as He or Ar to make the process pressure 1 atm. In the mixed gas, stable and high-density plasma is easily generated at atmospheric pressure. Since the partial pressure of the reactive gas is high, the oxidation rate is significantly increased. Moreover, employing a VHF electric field in AP plasma process, oscillation amplitudes of ionic species become smaller than those in RF plasma. The smaller oscillation amplitudes lead to the higher density of ions because they do not collide with the electrode surface, which results in the higher power density in the plasma. The kinetic energy of charged species is so small that ion induced damage in the film can be minimized. Also, the oscillation amplitude is small enough for electrons to be trapped in the small plasma gap between the electrode and Si surface, which enables the efficient input of plasma energy into the small volume and enhances the chemical reactions on the Si surface. Therefore, low-temperature ($T \leq 400°C$) prepared functional layers with high oxidation rates are expected to reduce the fabrication costs of oxide films.

References

[1] O. Schultz, S. W. Glunz and G. P. Willeke, Prog. Photovolt.: Res. Appl. **12** (2004) 553.

[2] S. Kimura, E. Murakami, T. Warabisako, E. Mitani and H. Sunami, J. Appl. Phys. **63** (1988) 4655.

[3] M. E. Vlachopouloua, P. Dimitrakisa, A. Tserepia, V. Em. Vamvakasa, S. Koliopouloua, P. Normanda, E. Gogolidesa and D. Tsoukalasb, Microelectronic Engineering **85** (2008) 1245–1247.

[4] Y. Yasuda, S. Zaima, T. Kaida and Y. Koide, J. Appl. Phys. **67** (1990) 2603.

[5] S. Gourrier, P. Friedel, P. Dimitriou and J. B. Theeten, Thin Solid Film **84** (1981) 379.

[6] J. B. Beck and J. Ruzyllo, Thin Solid Films **136** (1981) 173.

[7] E. D. Atanasova, K. I. Kirov and E. I. Kantardjeva, Phys. Status Solidi A **64** (1981) 73.

[8] S. S. Wong and W. G. Oldham, IEEE Electron Device Lett. **5** (1984) 155.

[9] V. Q. Ho and T. Sugano, Jpn. J. Appl. Phys. **19** (1980) 103.

[10] S. Taylor, G. P. Kennedy and W. Eccleston, Vacuum **38** (1988) 643.

[11] A. J. Choksi, R. La1 and A. N. Chandorkar, Solid Strate Electron **34** (1991) 765.

[12] K. Sekine, Y. Saito, M. Hirayama and T. Ohmi, IEEE Trans. Electron Devices **48** (2001) 1550.

[13] K. Takeda, S. Takashima, M. Ito and M. Hori, Appl. Phys. Lett. **93** (2008) 021501.

[14] S. Taylor, W. Eccleston and K. J. Barlow, J. Appl. Phys. **64** (1988) 6515

[15] Y. Z. Hu, J. Joseph and E. A. Irene, Appl. Phys. Lett. **59** (1991) 1353.

[16] I. Hasegawa, T. Yamauchi and H. Sugai, Jpn. J. Appl. Phys. **45** (2006) 1022.

[17] I. Hasegawa, T. Yamauchi and H. Sugai, Jpn. J. Appl. Phys. **46** (2007) 98.

[18] P. J. Jorgensen, J. Chem. Phys. **37** (1962) 874.

[19] N. F. Mott, Proc. R. Soc. London, Ser. A **376** (1981) 207.

[20] V. Q. Ho and T. Sugano, IEEE Electron Device Lett. **27** (1984) 1436.

[21] J. Perrière, N. Siejka, A. Remili, A. Laurent, A. Straboni and B. Vuillermoz, J. Appl. Phys. **59** (1986) 2752.

[22] C. Vinckier and De. S. Jaegere, J. Electrochem. Soc. **137** (1990) 628.

[23] K. J. Barlow and A. Kiermasz, IEE Electron. Lett. **21** (1985) 916.

[24] Martinet, R. A. B. Devine and M. Brunel, J. Appl. Phys. **81** (1997) 6996.

[25] W. Lerch, A. Gschwandtner, S. Schneider, T. Theiler, Z. Nenyei, B. Peuse and Y. Hu, Semicond. Sci. Technol. **24** (2009) 052001.

[26] M. Goto, K. Azuma, T. Okamoto and Y. Nakata, Jpn. J. Appl. Phys. **42** (2003) 7033.

[27] K. Saito, Y. Jin, T. Ono and M. Shimada, Jpn. J. Appl. Phys. **43** (2004) 765.

[28] B. E. Deal and A. S. Grove, J. Appl. Phys. **36 (**1965) 3770.

[29] S. A. Nelson and R. A. Burhmann, Appl. Phys. Lett. **50** (1987)1095.

[30] P. K. Hurley, J. F. Zhang, W. Eccleston and P. Coxon, Insulating Films on Semiconductors **1991** (Bristol: Adam Hilger).

[31] J. F. Zhang, S. Taylor, W. Eccleston and M. Nield, *Semicond. Sci. Technol.* **5** 1990824.

[32] M. Goerlitzer, P. Torres, N. Beck, N. Wyrsch, H. Keppner, J. Pohl and A .Shah, J. Non-Cryst. Solids **996** (1998) 227.

[33] F. Finger, P. Hapke, M. Luysberg, R. Carius, H. Wagner and M. Scheib, Appl. Phys. Lett. **65** (1994) 2588.

Chapter 3

Formation of SiO_2/Si structure with low interface state density by atmospheric-pressure VHF plasma oxidation

3.1 Introduction

In order to reduce the cost of crystalline silicon solar cells, the developmental trend of Si photovoltaics moves toward much thinner cells than 150 μm. Since the conversion efficiency of thin Si cells are strongly affected by the surface recombination of charged carriers, the formation of a high-quality SiO_2 passivation layer with a low interface state density (D_{it}) is a vital technology for thin Si cells [1-3]. Using high-temperature thermal oxidation processes (T>1000°C), SiO_2 layers with low D_{it} (of the order of 10^{10} $cm^{-2}eV^{-1}$) have been obtained on moderately-doped Si substrates. However, the high-temperature process may deteriorate the bulk Si quality and reduce the bulk carrier lifetime, especially for the lower quality Si materials [e.g., multi-crystalline Si or Czochralski Si (CZ-Si)] than float-zone Si [4]. Therefore, low temperature processing is desirable to obtain SiO_2 films with low D_{it} applicable for Si surface passivation. SiO_2 films with D_{it} of the order of 10^{10} $cm^{-2}eV^{-1}$ have been obtained by plasma enhanced chemical vapor deposition (PECVD) at (200 – 400°C) followed by a forming gas anneal [5,6]. Depending on the deposition conditions, however, the properties of SiO_2 films prepared by PECVD are affected by

impurities (H, N, H_2O, Si-OH groups), and are characterized by a higher porosity compared to SiO_2 films thermally-grown at higher temperatures [7]. Also the deposition of other dielectric films (SiN_x, Al_2O_3 etc.) has widely been studied for surface passivation of Si solar cells [8,9].

Other than the deposition methods, plasma oxidation that needs only O_2 and inert gas as plasma gases has attracted much attention as an alternative approach to prepare high-quality SiO_2 films. In nano-scale Si device processes, gate oxide films must be fabricated at low temperatures below 700°C to avoid undesirable diffusion-related and temperature-sensitive effects. Therefore, plasma oxidation process has been intensively investigated to realize ultra-large-scale integrated (ULSI) circuits [10].

Recently, we have studied the plasma oxidation of Si wafers to grow SiO_2 films using atmospheric-pressure (AP) plasma generated by a 150MHz very high frequency (VHF) electric field [11,12] and demonstrated that good quality SiO_2 films can be obtained using He/O_2 or Ar/O_2 plasma at low temperatures. In AP VHF plasma process, the kinetic energy of charged species is so small that ion induced damage in the film can be minimized. Also, the oscillation amplitude is small enough for electrons to be trapped in the small plasma gap between the electrode and Si surface, which enables the efficient input of plasma energy into the small volume and enhances the chemical reactions on the Si surface. Moreover, the AP plasma oxidation process is compatible for the open air process, which is very attractive for photovoltaic industry as a high-throughput oxidation process.

The objective of this research is to develop an AP plasma oxidation process of high-quality SiO_2/Si structures applicable for surface passivation of Si solar cells. As surface passivation films, the required properties for SiO_2 films are dense structure and low D_{it} comparable to those of high-temperature thermal oxides. Moreover, in contrast to the application for gate oxides in ULSI or thin film transistors, a high positive fixed oxide charge density (Q_f) is desirable for field-effect passivation of n-type Si surfaces.

3.2 Experimental details

Figure 3-1 shows a schematic illustration of an AP plasma oxidation apparatus used in this study. In the gap between the substrate and parallel-plate electrode, a stable plasma is generated at atmospheric pressure with 150MHz VHF power using a gas mixture of O_2 (0.5 – 5%) and He. The electrode is made of stainless steel plate coated with Al_2O_3, and its diameter is 50 mm. The oxidizing gas is introduced into the plasma region through a 1-mm-diameter hole at the center of the electrode.

The substrates used in the present experiments are n-type (001) oriented CZ-Si wafers (4 inch diameter) with the resistivity of 1 – 10 Ωcm. They were cleaned by a room temperature chemical cleaning method [13] and were finished by a diluted HF treatment. The oxidation temperature of Si wafer was varied in the range from 300 to 450°C by monitoring via a thermocouple embedded in the substrate heating stage. The plasma gap between the electrode and substrate was 0.8 – 1.0 mm. The VHF plasma power was varied in the range from 1000 to 1500 W. Detailed experimental conditions for Si oxidation are summarized in Table 3-1.

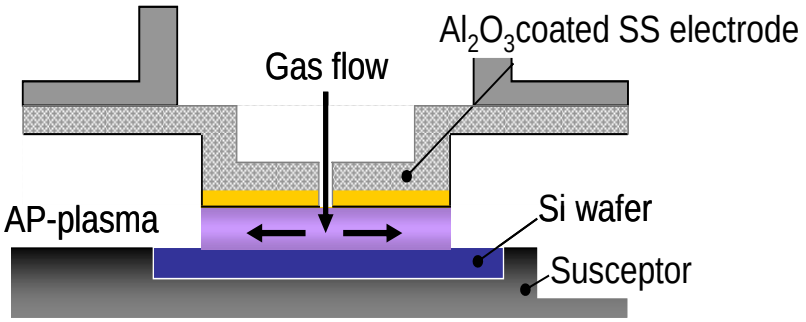

Fig.3-1 Schematic illustration of an AP plasma oxidation apparatus used in this study.

Table 3-1 Detailed experimental conditions for Si oxidation.

Process pressure (Torr)	760
O_2 concentration (%)	0.5 - 5
He flow rate (slm)	10 - 50
Plasma frequency (MHz)	150
Plasma power (W)	1000 - 1500
Plasma gap (mm)	0.8 - 1.0
Substrate temperature (°C)	300 - 450
Oxidation time (min)	1 - 25

Ellipsometry (Rudolph Auto EL III) with a wavelength of 632.8 nm was used to determine the thickness and refractive index of the oxide films. The oxide film structure was investigated by infrared absorption spectroscopy with a Fourier transform infrared absorption (FT-IR) spectrometer (Shimadzu FTIR-8600PC) in the wave number range of 400 – 4000 cm^{-1}. The depth profile of atomic composition was measured by X-ray photoelectron spectroscopy (XPS: ULVAC-PHI Quantum 2000). Cross sectional transmission electron microscopy (TEM: JEOL, JEM-2000FX) observations were performed to determine the microstructural

characteristics of SiO_2/Si interface. In order to characterize the interface electrical properties of oxide layers, Al/SiO_2/Si metal-oxide-semiconductor (MOS) capacitors were fabricated with 0.5-mm-diameter Al pads. The back contacting electrode at the rear Si surface was made by Al deposition. HF and QS capacitance–voltage measurements were performed using a 1 MHz C meter/CV plotter (HP 4280A) and quasistatic CV meter (Keithley 595). Some samples were subjected to a post-metallization annealing (PMA) in a forming gas (10%-H_2/N_2) for 30 min at 400°C, and at 760 Torr.

3.3 Results and discussion

Thickness profiles of SiO_2 layers prepared at 400°C for 25 min with different He gas flow rates of 10 and 50 L/min are shown in Fig.3-2. The position at 0 mm corresponds to the center of the plasma area where the gas-inlet hole (1 mm diameter) exists in the electrode (Fig.3-1). Therefore, no oxide is formed at the center due to the absence of plasma. This will become a problem, when the AP plasma oxidation is applied for processing large Si wafers. To solve this problem, it will be necessary to scan the substrate with a rectangular shaped electrode with a uniform gas-inlet slit instead of a gas-inlet hole at the center.

When the He flow rate is high at 50 L/min, the thickness increases gradually from the center along the radial direction. On the other hand, when the He flow rate is low at 10 L/min, the thickness variation becomes insignificant. The cause of the thickness variation is considered to be related with the gas residence time in the AP plasma. Since the gas flow velocity is highest at the center and becomes lower along the radial direction, the dissociation of O_2 molecules and the reaction time between O and Si surface is insufficient at the central area. Therefore, the oxide

thickness increases along the radial direction from the center for the higher He flow rate. When the He flow rate is 10 L/min, the gas residence time may be sufficient for oxidation in the central region.

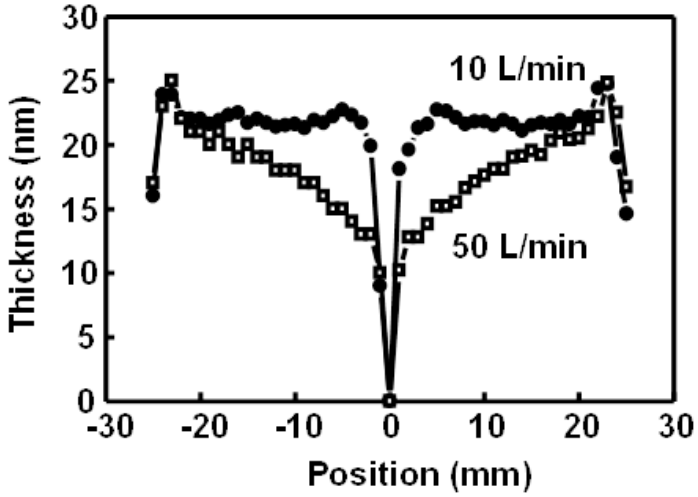

Fig.3-2 Thickness profiles of SiO_2 layers prepared at 400°C for 25 min with different He gas flow rates of 10 and 50 L/min. The position at 0 mm corresponds to the center of the plasma area where the gas-inlet hole (1 mm diameter) exists in the electrode.

Other than the above trend of thickness variation, we can notice humps in the thickness at the plasma edges in the center and the outer rim. These thickness humps are related with the electric field concentration at the sharp edges of the electrode at the center hole and the outer rim. By using the electrode of which edges are rounded off, we can obtain the oxide with fairly uniform thickness within 5 % variation as shown in Fig.3-3 (a). In this case, also the refractive index is almost uniform at about 1.46 corresponding to that of the thermal oxide grown at high temperatures (Fig. 3-3 (b)).

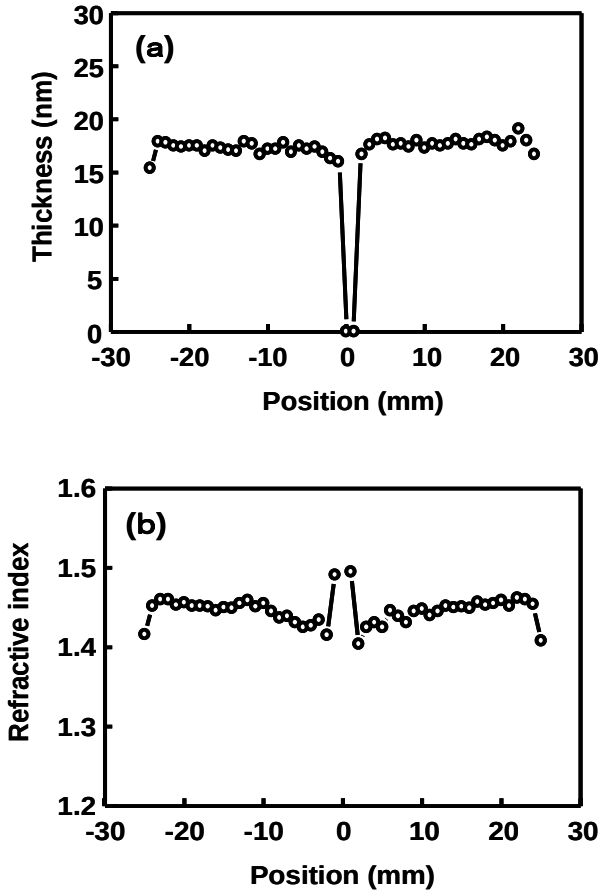

Fig.3-3 Fairly uniform thickness profile within 5 % (a) and refractive index (b) for SiO_2 formed by 16 min oxidation at 400°C.

Figure 3-4 shows experimental plots of the oxide thickness at the mid area between the wafer center and the periphery of the oxide film as a function of oxidation time *t*. In the case of thermal dry oxidation at 900°C [14], the initial oxidation rate is approximately 0.24 nm/min. Therefore, it can be said that the AP plasma oxidation at 400°C is apparently faster than the thermal oxidation. The feature of AP plasma oxidation curves in Fig.3-4 is that initially the oxide thickness increases at a high rate, and the growth slows down in the later oxidation stage. The activation energy of the average plasma oxidation rate was obtained to be approximately 0.22 eV. This value is about 10 times smaller than that of the thermal oxidation

process, which has been reported to be 2.01 eV [15] corresponding to that of the thermal diffusion of oxygen molecules in SiO_2. So, other mechanisms than the diffusion of oxygen molecules should be considered as the rate limiting process for plasma oxidation.

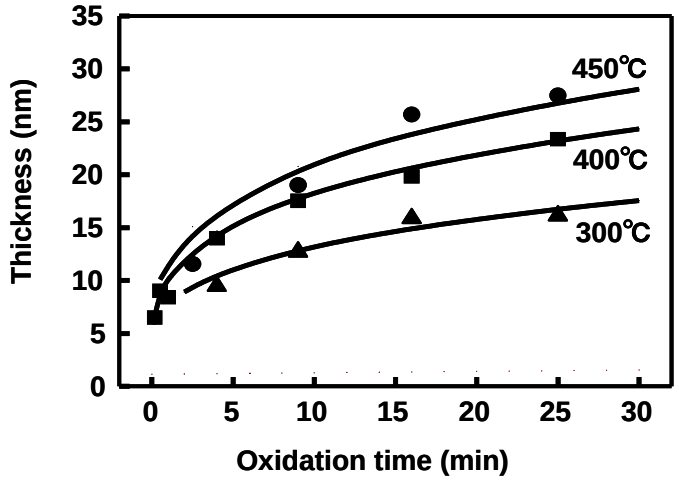

Fig.3-4 Experimental plots of the oxide thickness at the mid area between the wafer center and the periphery as a function of oxidation time *t*.

Recently, Hasegawa et al. [16,17] have shown that the key parameter for the plasma oxidation rate of Si is the electron density in their microwave plasma, and that the plasma oxidation mechanism can be explained based on the Jorgensen-Mott model [18,19] which assumes negative oxygen ions as transporting species. According to this model [16-19], the oxidation rate is enhanced by the electric field in the oxide layer due to the drift motion of the oxygen ions. Since the electric field decreases in time with increasing oxide thickness [16-19], the oxidation slows down in the later stage. So, this model may explain the feature of AP plasma oxidation curve that shows the retardation in the later stage and has much lower activation energy than that of the thermal oxidation which is limited by the diffusion of oxygen molecules. However, to clarify the

participation of oxygen ions as transporting species, further study on the effects of DC bias application on the plasma oxidation rate will be necessary.

Figure 3-5 shows XPS spectra in the Si 2*p* region for the SiO_2 layer formed by 1 %-O_2/He plasma oxidation for 25 min at 400°C. Si 2*p* peak observed at 99.7 eV is from the Si substrate [20]. In Fig.3-5, Si^{4+} peaks at 103.3 eV corresponding to SiO_2 structure are predominantly seen. A small sub-oxide component (Si^{1+}) is only seen in the bottom spectrum taken near the oxide/Si interface.

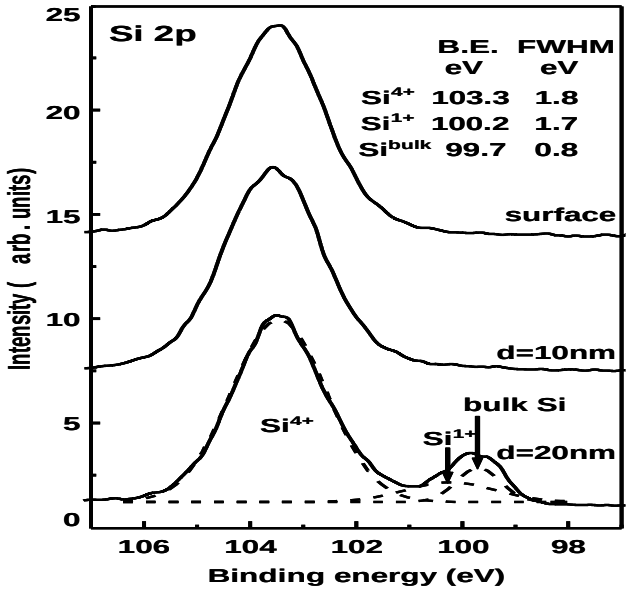

Fig.3-5 XPS spectra in Si 2*p* region for SiO_2 layer formed by 1 %-O_2/He plasma oxidation for 25 min at 400°C. *d* indicates the distance from the film surface. Bottom spectrum (*d* =20 nm) is taken from the region in close to the oxide/Si interface.

Figure 3-6 shows depth profiles of the film composition evaluated by XPS as a function of sputtering time. The chemical compositional percentages (the left axis) of the two elements O and Si in the oxide layer

are approximately 66% and 33%, respectively, which indicates the AP-plasma oxidized layer is a stoichiometric SiO_2.

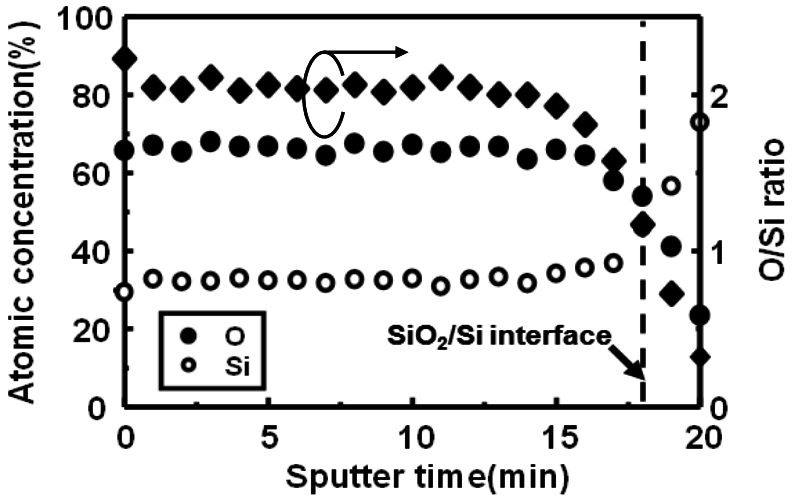

Fig.3-6 Depth profiles of the film composition also evaluated by XPS as a function of sputtering time.

Figure 3-7 shows a typical FT-IR absorption spectrum of the oxide layer in the wave number range from 400 to 1400 cm^{-1}. The asymmetrical and symmetrical vibration modes of Si-O-Si bonds are observed at the wave numbers of 1070 and 810 cm^{-1}, respectively. An absorption band due to the Si-O-Si rocking vibration is also observed at 455 cm^{-1}. The peak positions for thermally oxidized Si have been reported to be at 1076, 810 and 457 cm^{-1} [21], which are almost identical to those in the AP plasma oxide. The full width at half maximum (FWHM) of 1070 cm^{-1} peak in the AP plasma oxide is 81.1 cm^{-1}, which is also close to that in the thermal oxide (80.8 cm^{-1}). From these XPS and FT-IR results, it can be said that the SiO_2 film grown in the AP plasma has a dense structure similar to the thermal oxide.

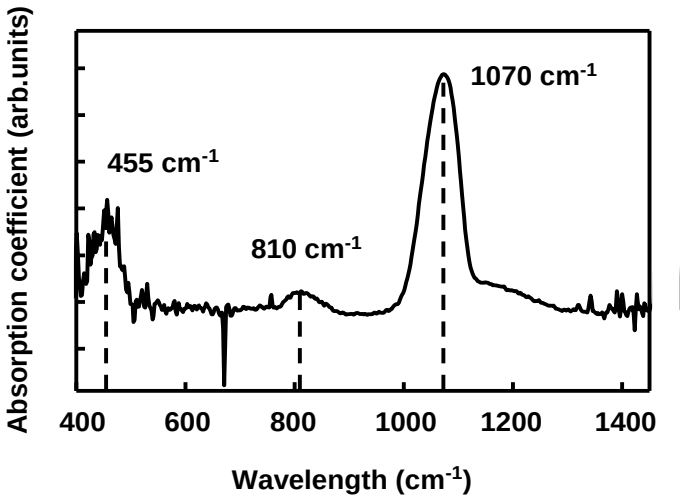

Fig.3-7 Typical IR absorption spectrum of oxide layer in wave number range from 400 to 1400cm^{-1}.

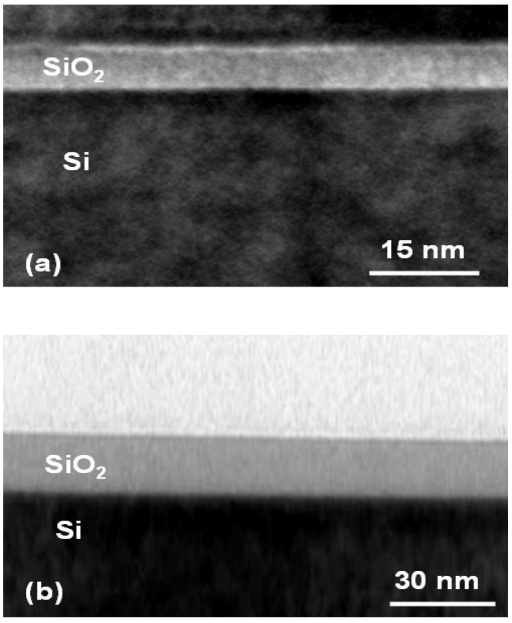

Fig.3-8 Cross sectional TEM images of SiO_2/Si structure formed at 400 °C for (a) 1 min and (b) 16 min oxidation.

Figure 3-8 (a) and (b) show cross sectional TEM images of SiO_2/Si structure formed at 400 °C for 1 min and 16 min oxidation, respectively.

The very flat interface is clearly discerned in each micrograph. Therefore, by using the AP plasma oxidation technique, we can obtain a sharp interface between SiO_2 film and Si substrate even at 400 °C with a very short oxidation time (1 min).

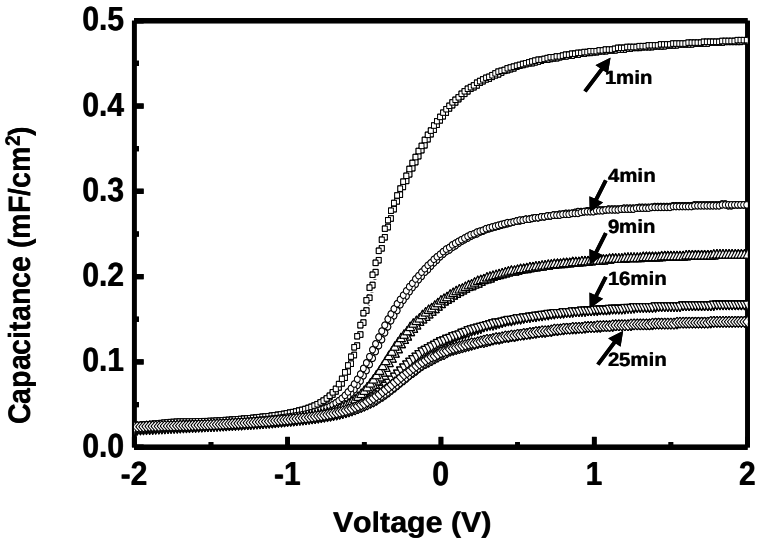

Fig.3-9 Typical HF *C–V* curves with various thickness of SiO_2 layer formed by 0.5% O_2/He plasma at 400°C.

Finally, systematic measurements of HF *C–V* characteristics of MOS capacitors fabricated on AP plasma oxidized Si were performed to investigate the effect of different oxidation parameters on D_{it} and Q_f of the SiO_2 films. Figure 3-9 shows typical HF *C–V* curves with the varying oxidation time for SiO_2 layer formed by 0.5% O_2/He plasma at 400°C. All the measured *C–V* curves showed no hysteresis or hump. The capacitance in the accumulation region decreases with increasing oxidation time due to the thickening of the SiO_2 layer. D_{it} and Q_f have been estimated by Terman's method [22] and from the flat-band voltage shift, respectively, and summarized in Fig.3-10. D_{it} and Q_f gradually decrease with increasing oxidation time. The PMA has little effect on Q_f for longer oxidation times

than 9 min and Q_f remains in the range of (4 - 6) × 10^{11} cm^{-2}. On the other hand, after the PMA, D_{it} decreased below the determination limit of the Terman's method. Probably, the hydrogen termination of the dangling bonds and structural relaxation at the SiO_2/Si interface are responsible for the decrease in D_{it} similarly to the thermal oxide case.

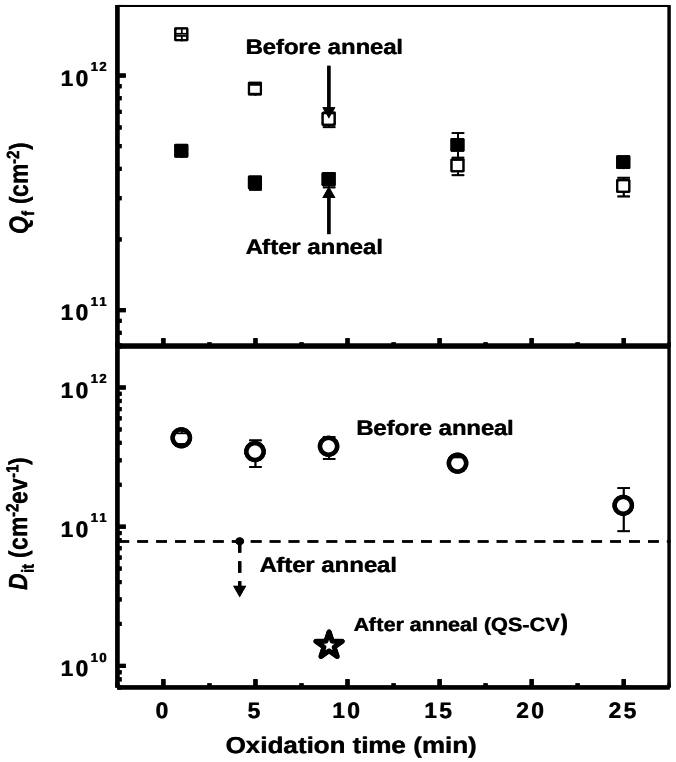

Fig.3-10 D_{it} and Q_f as a function of oxidation time. After PMA, D_{it} decreased below the determination limit of Terman's method.

As the more reliable measurements for low D_{it} case, the HF and QS *C*–*V* curves for the same MOS capacitor as in Fig.3-11 (*t* = 9 min with PMA) have been measured, and the result is shown in Fig.3-12. The D_{it} was determined using the following equation [22]:

$$D_{it} = C_{OX} / q\{(C_{QS} / C_{OX}) / [1 - C_{QS} / C_{OX}] - (C_{HF} / C_{OX}) / [1 - C_{HF} / C_{OX}]\}$$

in which C_{OX} is the oxide capacitance, q is the elemental charge, C_{QS} is the quasi static capacitance and C_{HF} is the high frequency capacitance.

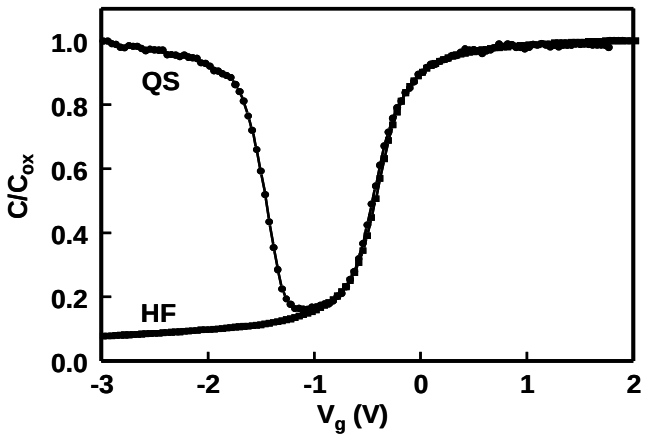

Fig.3-11 HF and QS *C–V* curves for MOS capacitor for 17.4-nm-thick SiO_2 (t = 9 min) after PMA.

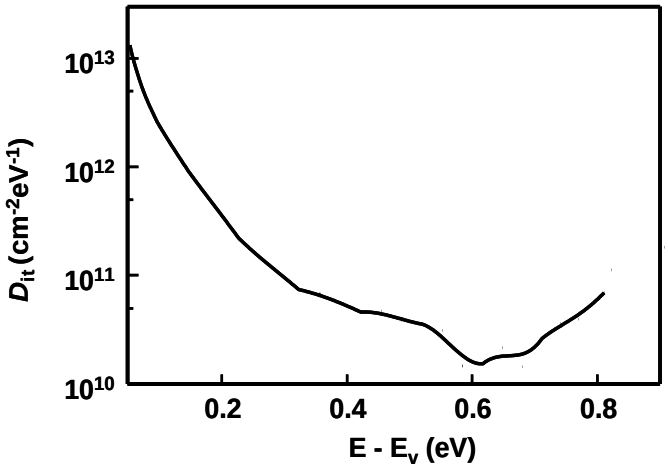

Fig.3-12 Energy distribution of interface state density in energy band gap calculated from HF and QS *C–V* curves. D_{it} around mid gap is approximately 1.4×10^{10} $cm^{-2}eV^{-1}$.

The energy distribution of D_{it} in the band gap is calculated from the HF and QS *C–V* curves as shown in Fig.3-12, which shows a minimum value of D_{it}

= 1.4 × 10^{10} $cm^{-2}eV^{-1}$. This value is comparable to that SiO_2/Si interfaces thermally grown at about 1000 °C. On the other hand, Q_f = 5.3 × 10^{11} cm^{-2} obtained in this sample is much higher than that in thermal oxide grown at high temperatures [2], which is a general feature for plasma oxides [5-9]. Although the reason for high Q_f in AP-plasma oxide is not clear at present, one of the possible reasons may be related with UV-irradiation induced traps in the AP-plasma oxides. From the view point of surface passivation, the presence of a high positive fixed charge density is useful for field-effect passivation of n-type Si surfaces. An effective surface recombination velocity (S_{eff}) can be estimated using the experimental D_{it} distribution (Fig. 11) and Q_f = 5.3 × 10^{11} cm^{-2} based on the Schockley-Read-Hall surface recombination model [23]. The estimated S_{eff} for n-doping of 10^{16} cm^{-3} under the low level injection condition was below 10 cm/s, which is low enough to realize high-efficiency Si solar cells [24,25]. Therefore, it can be said that the AP plasma oxidation technique is quite promising for surface passivation of Si wafers.

3.4 Conclusions

In this work, we have investigated the effects of formation conditions on the properties of SiO_2/Si structure fabricated by oxidation of n-type Si substrates using AP plasma. Oxidation rates for AP plasma oxidation at 400°C are faster than those by thermal dry oxidation at 900°C. From the characterization results of ellipsometry, XPS, FT-IR and TEM, it can be said that the AP plasma oxidation technique is capable of producing high-quality SiO_2/Si structures comparable to those of high-temperature

thermal oxides. Moreover, by optimizing the formation conditions together with a post-metallization annealing, the SiO_2/Si structure with low D_{it} of 1.4×10^{10} $cm^{-2}eV^{-1}$ around the midgap and moderately high Q_f of 5.3×10^{11} cm^{-2} is achieved. These characteristics (low D_{it} and high Q_f) is useful to realize effective field-effect passivation of Si surfaces for photovoltaic application.

References

[1] M. A. Green, Prog. Photovoltaics **7** (1999) 327.

[2] M. J. Kerr, and A. Cuevas, Semicond. Sci. Technol. **17** (2002) 35.

[3] T. Jana, S. Mukhopadhyay, and S. Ray, Sol. Energy Mater. Sol. Cells **71** (2002) 197.

[4] O. Schultz, S. W. Glunz, and G. P. Willeke, Prog. Photovolt.: Res. Appl. **12** (2004) 553.

[5] Z. Chen, K. Yasutake, A. Doolittle, and A. Rohatgi, Appl. Phys. Lett. **63** (1993) 2117.

[6] Y. Hiroshige, S. Higashi, K. Matsumoto, and S. Miyazaki, Jpn. J. Appl. Phys. **49** (2010) 08JJ01.

[7] P. Paneka, K. Drabczyk, A. Focsa, and A. Slaoui, Mater. Sci. Eng. B **165** (2009) 64.

[8] K. J. Weber, and H. Jin, Appl. Phys. Lett. **94** (2009) 063509.

[9] P. Saint-Cast, D. Kania, M. Hofmann, J. Benick, J. Rentsch, and R. Preu, Appl. Phys. Lett. **95** (2009) 151502.

[10] W. Lerch, A. Gschwandtner, S. Schneider, T. Theiler, Z.Nenyei, B. Peuse, and Y. Hu, Semicond. Sci. Technol. **24** (2009) 052001.

[11] H. Kakiuchi, H. Ohmi, M. Harada, H. Watanabe, and K. Yasutake, Appl. Phys. Lett. **90** (2007) 091909.

[12] H. Kakiuchi, H. Ohmi, M. Harada, H. Watanabe, and K. Yasutake, Appl. Phys. Lett. **90** (2007) 151904.

[13] T. Ohmi, J. Electrochem. Soc. **143** (1996) 2957.

[14] B. E. Deal, and A. S. Grove, J. Appl. Phys. **36** (1965) 3770.

[15] G. Gerlach, K. Maser, and A. M. Saad, Phys. Stat. Solidi B **246** (2009) 2242.

[16] I. Hasegawa, T. Yamauchi, and H. Sugai, Jpn. J. Appl. Phys. **45** (2006) 1022.

[17] I. Hasegawa, T. Yamauchi, and H. Sugai, Jpn. J. Appl. Phys. **46** (2007) 98.

[18] P. J. Jorgensen, J. Chem. Phys. **37** (1962) 874.

[19] N. F. Mott, Proc. R. Soc. London, Ser. A **376** (1981) 207.

[20] J. S. Johannessen, W. E. Spicer, and Y. E. Strausser. J. Appl. Phys. **47** (1976) 3028.

[21] C. T. Kirk, Phys. Rev. B. **38** (1988) 1255.

[22] E. H. Nicolian, J. R. Brews, MOS (Metal Oxide Semiconductor) Physics and Technology (Wiley, New York, 1982).

[23] K. Yasutake, Z. Chen, S. K. Pang, and A. Rohatgi, J. Appl. Phys. **75** (1994) 2048.

[24] J. D. Arora, S. N. Singh, and P. C. Mathur, Sol. Stat. Elclron. **24** (1981) 739.

[25] V. Perraki, Solar Energy Mater. Sol. Cells **94** (2010) 1597.

Chapter 4

Interface properties of SiO_xN_y layer on Si prepared by atmospheric-pressure plasma oxidation-nitridation

4.1 Introduction

Silicon oxynitride (SiO_xN_y) is very useful material for applications in microelectronic and optoelectronic devices due to the possibility of tailoring the film composition and property according to O/N ratio. Recently, considerable attention has been focused on SiO_xN_y for anti-reflection coatings and surface passivation films for thin crystalline Si solar cells [1-3]. It has been reported that SiO_xN_y films with high positive fixed charge density (Q_f) in the range of 10^{12} cm^{-2} is effective for field effect passivation of n-type Si surfaces [2].

So far, several methods have been applied to grow SiO_xN_y films. For example, high temperature (T > 900°C) processes such as the direct thermal oxyntridation of Si in NO or N_2O ambient [4,5] and the annealing of SiO_2 in nitrogen containing ambient [6,7] have been widely used. However, the high temperature processes suffer a large thermal budget and a redistribution problem of dopant atoms. Plasma-enhanced chemical-vapor deposition (PECVD) process is a low-temperature alternative below 400°C [8-10]. However, PECVD method needs toxic precursor gases, and it is also noted that the interfacial properties prepared by this method are usually inferior to those of thermal oxides [11], because the deposition method does not consume the substrate Si unlike thermal oxidation.

Moreover, in the films prepared by the low-temperature PECVD, the concentration of hydrogen atoms in the form of Si–OH and Si–H bonds is high, which are responsible for poor dielectric properties [12]. Nitridation of silicon oxide in low-pressure nitrogen plasma has also been investigated to fabricate SiO_xN_y at low temperatures [13,14]. In the case of low-pressure nitrogen plasma, the ion bombardment of the film surface is a serious problem to develop highly reliable ultra-large-scale integrated circuits (ULSI) [15]. Recently, we have studied the plasma oxidation of Si wafers to grow SiO_2 films using atmospheric-pressure (AP) plasma generated by a 150MHz very high-frequency (VHF) electric field and demonstrated that high-quality SiO_2 films can be obtained using He/O_2 or Ar/O_2 plasma at 400°C [16,17]. We have also reported that the AP VHF plasma oxidation process at 400°C is capable of producing material quality of SiO_2 films comparable to those of high-temperature (T > 1000°C) thermal oxides. The SiO_2/Si structure with low interface state density (D_{it}) around the midgap of 1.4×10^{10} $cm^{-2}eV^{-1}$ and moderately high Q_f of 5.3×10^{11} cm^{-2} has been demonstrated [18]. Therefore, N addition into the SiO_2 film by AP plasma oxidation-nitridation using O_2 and N_2 precursor gas mixture is an alternative approach for obtaining SiO_xN_y films at a low temperature of 400°C.

The purpose of this work is to present method for preparing SiO_xN_y films by AP VHF plasma oxidation-nitridation with a detailed analysis of interface properties of SiO_xN_y layer by capacitance–voltage (*C*–*V*) measurements on metal–SiO_xN_y–Si capacitors.

4.2 Experimental details

The details of the AP VHF plasma apparatus have been reported

previously [18]. A schematic illustration of an electrode for AP VHF plasma oxidation-nitridation is shown in Fig.4-1. In the gap between the substrate and parallel-plate electrode, stable plasma is generated at atmospheric pressure with 150MHz VHF power using a gas mixture of 1%-O_2/He. N_2 gas was simultaneously introduced into the AP VHF plasma with gas flow rates of 1, 10 and 100 sccm. The N_2/O_2 gas flow ratios were 0.01, 0.1 and 1. The temperature of Si wafer was fixed at 400°C by monitoring by a thermocouple embedded in the substrate heating stage. The detailed experimental conditions are shown in Table 4-1.

The substrates used in the present experiments were n-type (001) CZ-Si wafers (4 inch diameter) with the resistivity of 1–10 Ωcm. They were cleaned by a room temperature chemical cleaning method [19] and were finished by a diluted HF treatment. After AP plasma oxidation-nitridation, some of the samples were subjected to a forming gas anneal (FGA) in 10%-H_2/He for 30 min at 400 °C. In order to investigate Q_f and D_{it} of SiO_xN_y film, Al/SiO_xN_y/Si metal-oxide-semiconductor (MOS) capacitors were fabricated with 0.5-mm-diameter Al pads by vacuum deposition. Back contacting electrode at the rear Si surface was also made by Al deposition.

The thickness of SiO_xN_y layer was determined by ellipsometry (Rudolph Auto EL III) with a wavelength of 632.8 nm. The chemical bonding in the material was investigated by Fourier transform infrared absorption (FT-IR) spectrometry (Shimadzu FTIR–8600PC) in the wave number range of 400–4000 cm^{-1}. X-ray photoelectron spectroscopy (XPS: ULVAC-PHI Quantum 2000) was used to investigate the depth profile of atomic composition and bonding of atoms in SiO_xN_y films. High-frequency (HF) and quasistatic (QS) *C–V* measurements were performed using a 1 MHz C

meter/CV plotter (HP 4280A) and quasistatic CV meter (Keithley 595), respectively.

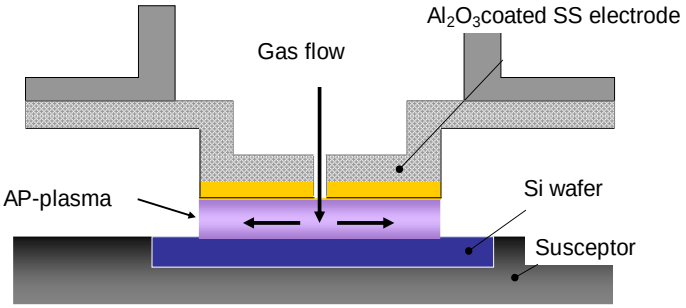

Fig.4-1 Schematic illustration of an AP VHF plasma oxidation-nitridation apparatus used in this study. The electrode is made of stainless steel plate coated with Al_2O_3, and its diameter is 50 mm.

Table 4-1 Oxidation-nitridation conditions for Si wafers.

Pressure (Torr)	760
O_2 concentration (%)	1 - 5
O_2 flow rate (sccm)	100
N_2 flow rate (sccm)	1.10,100
VHF (MHz)	150
VHF power (W)	1000 - 1500
Plasma gap (mm)	0.8 - 1
Substrate temperature(°C)	400
Oxidation time (min)	9 - 25

4.3 Results and discussion

Thickness of films prepared at 400°C for 9 min under different N_2/O_2 flow ratios of 0.01, 0.1 and 1, was 20.8, 19.5 and 18.9 nm, respectively. (The film thickness was a mean value for measurements of 8 different sites on the sample.) Since the difference in the film thickness is small (< ±5%), its effect on the interface state properties may be negligible. Figure 2 shows

FTIR spectra of the films prepared at 400°C for 9 min under different N_2/O_2 flow ratios. The dotted lines in Figure 2 indicate the stretching and bending vibration modes of Si–O–Si bonds at the wave numbers of 1075 and 810 cm^{-1}, respectively. Almost no apparent peak for Si–N stretching mode at 835 cm^{-1} is observed [1], which may be related with the larger dissociation energy of N_2 than that of O_2 molecules.

In Fig.4-2, the strongest peak in IR spectra corresponds to Si–O–Si stretching mode, indicating that the film consists predominantly of SiO_2. The dielectric constant of the film was calculated using the maximum accumulation capacitance obtained by C-V curves. The result showed that the dielectric constant was fairly uniform over the sample area with the variation of about 2 %, and that the average dielectric constants of the films were 4.26 and 4.01 for N_2/O_2 flow ratios of 0.01 and 1, respectively. Since the dielectric constants of SiO_2 and Si_3N_4 are 3.9 and 7.5, respectively, nitrogen atoms are considered to be incorporated in the SiO_2 structure.

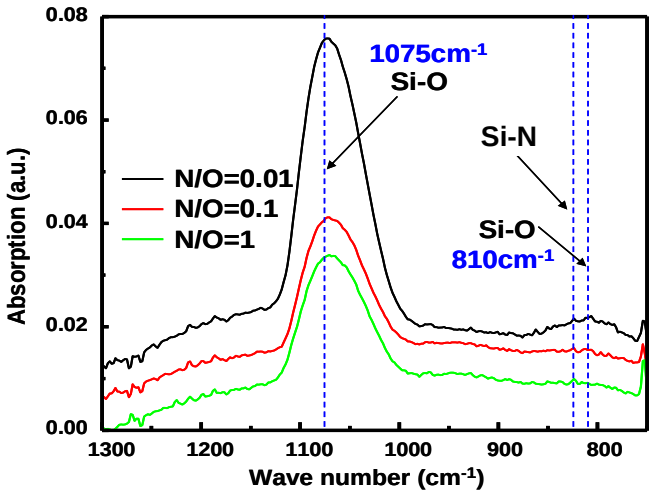

Fig.4-2 IR spectra of films prepared by AP VHF plasma oxidation-nitridation process under different N_2/O_2 gas flow ratios of 0.01, 0.1 and 1.

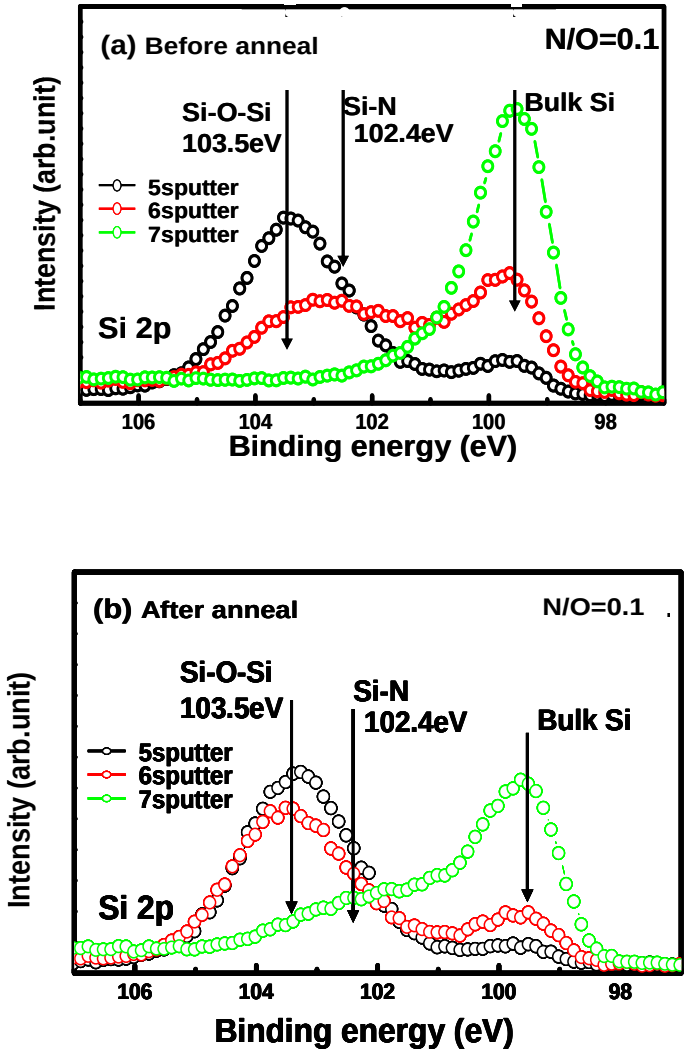

Fig.4-3 XPS spectra in the Si 2*p* region for the SiO_xN_y layer formed by 1%-O_2/He AP plasma oxidation-nitridation process at 400°C for 9 min with N_2/O_2 gas flow ratio of 0.1. (a) As-grown sample. (b) After annealed sample, respectively.

XPS spectra in the Si 2*p* region for the SiO_xN_y layer formed at 400°C for 9 min with N_2/O_2 gas flow ratio of 0.1 are shown in Fig.4-3. The Si 2*p* peak observed at 99.7 eV is from the Si substrate and the one at 103.5 eV from Si–O–Si bonding. On the as-grown sample, as shown in Fig.4-3 (a), after 5 times of surface-layer sputtering by 10 keV Ar ions (duration of one

sputtering is 10 sec), Si–O–Si bonding peak is strong but a small peak from the Si substrate is also seen. By 6th and 7th sputtering, Si–O–Si peak decreases and bulk Si peak increases. It is noteworthy that Si–N bonding at 102.4 eV is also detected. Since the Si–N peak becomes clear before the Si–O–Si peak vanishes, Si-N bonding is supposed to be located at the SiO_2/Si interface region. On the annealed sample, as shown in Fig.4-3 (b), the decrease of Si–O–Si peak after 6th sputtering is not significant as that in the as-grown sample and the Si–O–Si peak still remains after 7th sputtering. The Si–N peak becomes well observable after 7th sputtering in the annealed sample instead of 6th sputtering for the as-grown case. However, the tendency of decreasing Si–O–Si peak and increasing bulk Si peak with increasing sputtering time is the same for both as-grown and annealed samples. These results can be understood by considering the increase in SiO_2 thickness by the annealing and the presence of Si-N bonding at the SiO_2/Si interface region. The thickness increase in the annealed SiO_2 sample is considered to be due to the density relaxation of SiO_2 by the thermal annealing [20,21].

Figure 4-4 shows depth profiles of Si, O and N atom concentrations in SiO_xN_y films measured by XPS as a function of sputtering time, which reveals that incorporated N atoms (~4%) locate at the film/substrate interface for all the samples. These results are similar to those by the high-temperature process, such as the direct thermal oxyntridation of Si in N_2O ambient at 1000°C [5]. According to the thermodynamics of Si–N–O system, nitrogen in bulk SiO_2 is not thermodynamically stable but may be stable at the interface [22], therefore, it has been assumed that nitrogen incorporated into the film during oxynitridation (especially in high-temperature N_2O or NO process) reacts only with Si–Si bonds at or

near the interface, not with Si–O bonds in the bulk of the SiO_2 overlayer. Similarly, we suppose that since the dissociation of nitrogen molecules is not significant in the present case, nitrogen migrates to the Si/SiO_2 interface during AP plasma oxidation-nitridation.

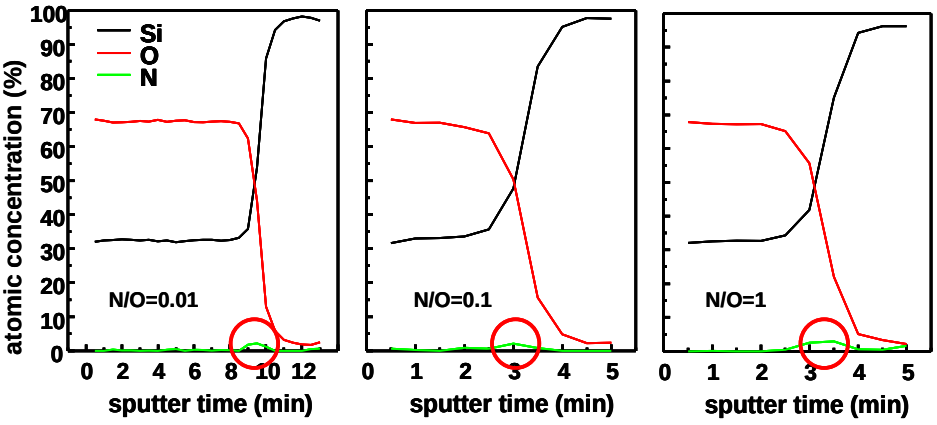

Fig.4-4 XPS depth profiles of Si, O and N concentrations in SiO_xN_y layers prepared by AP VHF plasma oxidation-nitridation process under different N_2/O_2 ratios.

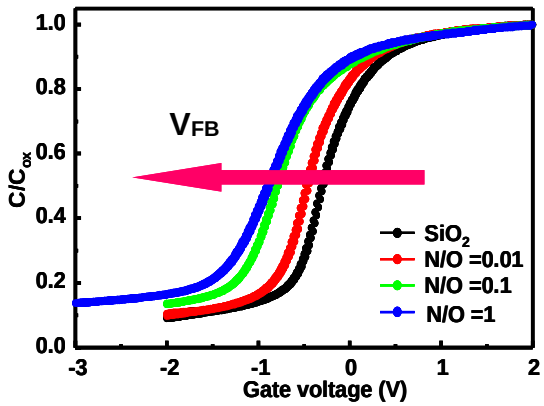

Fig.4-5 Typical HF *C–V* curves for $Al/SiO_xN_y/Si$ capacitors utilizing SiO_xN_y layers prepared by different N_2/O_2 flow ratios. The *C–V* curve shifts to a negative gate bias direction with increasing N_2/O_2 ratio.

Finally, interface electrical quality of SiO_xN_y layers prepared by AP VHF plasma oxidation-nitridation process has been investigated. Figure 4-5

shows typical HF *C–V* curves of the MOS capacitors utilizing SiO_xN_y layers formed by various N_2/O_2 flow ratios. The HF *C–V* curve shifts to a negative gate bias direction with increasing N_2/O_2 flow ratios, which shows an increase in positive Q_f with incorporation of more N atoms into the SiO_2 film (Fig.4-4). The value of Q_f have been estimated by flat-band voltage shift to be 5.1×10^{11}, 8.1×10^{11} and 8.4×10^{11} cm^{-2} for N_2/O_2 flow ratios of 0.01, 0.1 and 1, respectively.

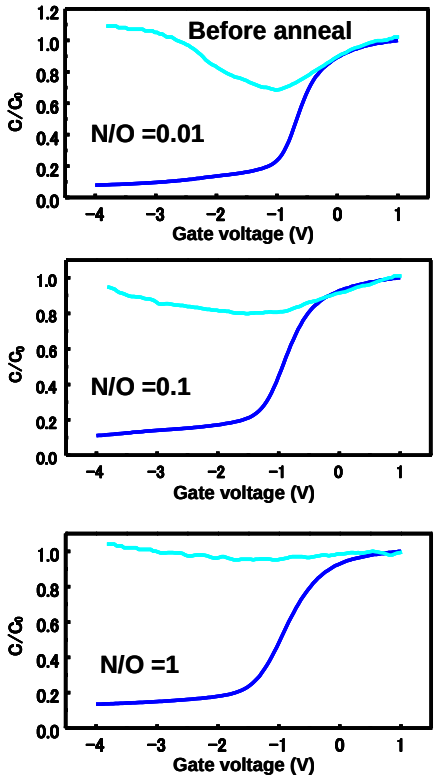

Fig.4-6 HF and QS C–V curves for Al/SiO_xN_y/Si MOS capacitors (before anneal) utilizing SiO_xN_y layers prepared by various N_2/O_2 gas flow ratios of 0.01, 0.1 and 1.

The HF and QS *C–V* curves for Al/SiO_xN_y/Si MOS capacitors before and after FGA are shown in Fig.4-6 and Fig.4-7, respectively. The annealed Al/SiO_xN_y/Si MOS capacitors show better interface properties compared with those without FGA. D_{it} after FGA were 6.1×10^{11}, 1.2×10^{12} and 2.3×10^{12} $cm^{-2}eV^{-1}$ for N_2/O_2 flow ratio of 0.01, 0.1 and 1, respectively. It is well

known that an introduction of a small amount of nitrogen into the SiO_2 gate oxide lead to an enhanced defect density in the case of N pileup at the Si/SiO_2 interface [23]. From our XPS results, when N_2/O_2 gas flow ratio increases, the more N atoms pileup at the Si/SiO_2 interface during AP plasma oxidation-nitridation, therefore, D_{it} increases largely with increasing N_2/O_2 flow ratio from 0.01 to 1. The corresponding values of Q_f were 1.2×10^{12}, 1.4×10^{12} and 1.5×10^{12} cm^{-2}, respectively. It is noted that D_{it} decreases largely with decreasing N_2/O_2 flow ratio from 1 to 0.01, while the decrease of Q_f is insignificant. These results suggest that significantly low N_2/O_2 flow ratio is a key parameter to achieve a small D_{it} and relatively large Q_f, which is effective for field effect passivation of n-type Si surfaces.

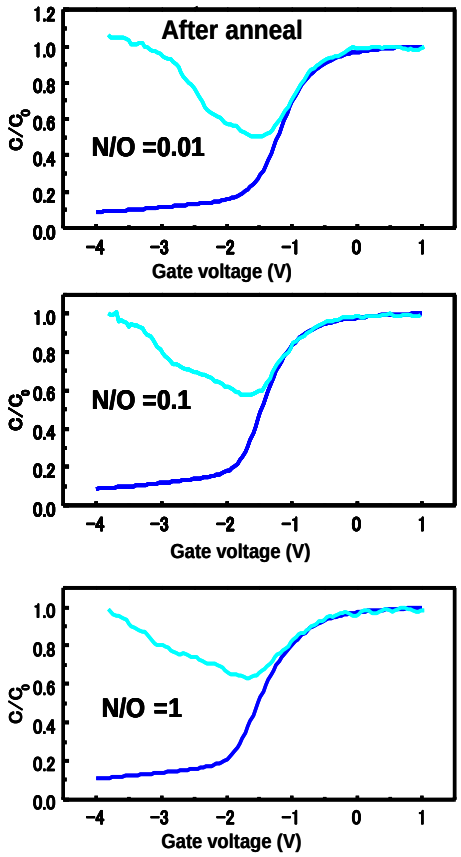

Fig.4-7 HF and QS C–V curves for $Al/SiO_xN_y/Si$ MOS capacitors (after anneal) utilizing SiO_xN_y layers prepared by various N_2/O_2 gas flow ratios of 0.01, 0.1 and 1.

4.4 Conclusions

SiO_xN_y films with a low nitrogen concentration (~4%) have been prepared on n-type (001) Si wafers at 400°C for 9 min by oxidation-nitridation process in AP plasma using O_2, N_2 diluted in He gas. Interface properties of SiO_xN_y films have been investigated by *C–V* measurements, and it is found that addition of N into the oxide increases both the values of D_{it} and Q_f. After FGA, D_{it} at midgap decreases from 2.3 $\times$ 10^{12} to 6.1 $\times$ 10^{11} $cm^{-2}eV^{-1}$ with decreasing N_2/O_2 flow ratio from 1 to 0.01, while the decrease of Q_f is insignificant from 1.5 $\times$ 10^{12} to 1.2 $\times$ 10^{12} cm^{-2}. These results suggest that low N_2/O_2 flow ratio is a key parameter to achieve a low D_{it} and relatively high Q_f, which is useful to realize an effective field effect passivation of n-type Si surfaces.

References

[1] J. Dupuis, E. Fourmond, J. F. Lelievre, D. Ballutaud and M. Lemiti, Thin Solid Films **516** (2008) 6954.

[2] J. Seiffe, L. Gautero, M. Hofmann, J. Rentsch, R. Preu, S. Weber and R. A. Eichel, J. Appl. Phys. **109** (2011) 034105.

[3] B. Hallam, B. Tjahjono, and S. Wenham *Sol. Energy Mater. Sol. Cells* **96** (2012) 173.

[4] E. P. Gusev, H. C. Lu, T. Gustafsson, E. Garfunkel, M. L. Green and D. Brasen, J. Appl. Phys. **82** (1997) 1997.

[5] H. C. Lu, E. Gusev, N. Yasuda, M. Green, G. Alers, E. Garfunkel and T. Gustafsson, Appl. Surf. Sci. **166** (2000) 465.

[6] T. Hori, T. Yasui and S. Akamatsu, IEEE Trans. Electron Dev. **39** (1992) 134.

[7] Z. Q. Yao, H. B. Harrison, S. Dimitrijev and Y. Yeow, IEEE Electron Dev. Lett. **16** (1995) 345.

[8] Z. Yu, M. Aceves, J. Carrillo and R. Estopier, Thin Solid Films **515** (2006) 2366.

[9] D. Criado, A. Zuniga and I. Pereyra, J Non-Crys Solids **354** (2008) 2809.

[10] K.F. Albertin and I. Pereyra, J Non-Crys Solids **354** (2008) 2646.

[11] M. L. Green, E.P. Gusev, R. Degraeve and E.L. Garfunkel, J.Appl. Phys. **90** (2001) 2057.

[12] I. Pereyra and M.I. Alayo, J Non-Crys Solids **212** (1997) 225.

[13] S. Murakawa and S. Ishizuka, T. Nakanishi, T. Suwa, A. Teramoto, S. Sugawa, T. Hattori and T. Ohmi, Jpn. J. Appl. Phys. **49** (2010) 091301.

[14] R. Kraft, TP. Schneider, WW. Dostalik and S. Hattangady, J Vac Sci Technol B **15** (1997) 967.

[15] R. Perera, A. Ikeda, R. Hattori and Y. Kuroki, Thin Solid Films **423** (2003) 212.

[16] H. Kakiuchi, H. Ohmi, M. Harada, H. Watanabe and K. Yasutake, Appl. Phys. Lett. **90** (2007) 151904.

[17] H. Kakiuchi, H. Ohmi, M. Harada, H. Watanabe and K. Yasutake, Appl. Phys. Lett. **90** (2007) 091909.

[18] Z. Zhuo Y. Sannomiya, K. Goto, T. Yamada, H. Ohmi, H. Kakiuchi and K. Yasutake, Curr. Appl. Phys. **12** (2012) S57.

[19] T. Ohmi, J. Electrochem. Soc. **143** (1996) 2957.

[20] K. Taniguchi, M. Tanaka, C. Hamaguchi and K. Imai, J. Appl. Phys. **67** (1990) 2195.

[21] K. Tatsumura, T. Watanabe, D. Yamasaki, T. S himura, M. Umeno and I. Ohdomari, Jpn. J. Appl. Phys. **42** (2003) 7250.

[22] E. P. Gusev, H. C. Lu, E. L. Garfunkel, T. Gustafsson and M.L. Green, IBM. J. Res. Dev. **43** (1999) 265.

[23] K. Watanabe, T. Tatsumi, M. Togo and T. Mogami, J. Appl. Phys. **90** (2001) 4701.

Chapter 5

Characterization of AlO_x thin films prepared by AP VHF plasma oxidation

5.1 Introduction

5.1.1 Aluminum oxide

Aluminum oxide (Al_2O_3) is one of the simplest ionic oxides and also an amphoteric oxide. Corundum or α-Al_2O_3 (trigonal) is the most commonly occurring crystalline form. In the α-Al_2O_3 crystal structure, oxygen ions nearly form a hexagonal close-packed structure with aluminum ions filling two-thirds of the oxygen octahedron. Alumina is also known to exist in several other crystalline phases, namely γ (cubic spinel), δ (either tetragonal or orthorhombic), η (cubic spinel), θ (monoclinic), β (hexagonal), and κ-alumina (orthorhombic) [1-3].

Aluminum oxide has a large bandgap of 8.8 eV and a high dielectric constant of 9 [4], and has other excellent inherent properties such as high mechanical strength, chemical and thermal stability, high electrical resistivity, durability against hostile environments and high transparency down to 250 nm. Al_2O_3 films can be deposited by physical or chemical methods, and actually find several applications in different areas of technological research. For example, Al_2O_3 films have been widely used for their practical applications in microelectronic devices [5], optoelectronics [6], sensors [7] and surface passivation of solar cells [8].

Under normal processing conditions ($T \leq 350°C$), Al_2O_3 is amorphous, although γ-alumina may form at high temperatures ($T > 700°C$). The

previous studies reported that Al_2O_3 thin films prepared by the atomic layer deposition (ALD) and by the physical vapor deposition (PVD) were amorphous [9].

5.1.2 Formation of AlO_x films by AP VHF plasma oxidation

Within the trend towards thinner and more efficient silicon solar cells, surface passivation is becoming a more and more important issue. At the crystalline silicon surface, the abrupt discontinuity in the crystal structure results in a high density of dangling bonds, creating a large density of defects in the bandgap. Passivation schemes allow terminating these dangling bonds properly, and as a consequence, the number of recombination centers can be considerably decreased. SiO_2 and SiN_x are the standard surface passivation materials. SiO_2 and SiN_x have all inherent advantages and drawbacks. SiO_2 yields the lowest interface state densities [10] but only when grown at high temperatures (~ 950 – 1100°C) followed by a subsequent anneal. SiN_x is an excellent antireflection coating and is grown at lower temperatures ($T \leq 400$°C), but because of the high positive fixed charge density (Q_f), the effectiveness of the passivation depends on the Si doping type and level.

A next generation prototype material for surface passivation is Al_2O_3. The main benefit is that due to a high negative Q_f in the range of (10^{12} – 10^{13}) cm^{-2} in combination with a moderate interface state density (D_{it}) of (10^{10} – 10^{12}) $eV^{-1}cm^{-2}$, a low surface recombination velocity can be achieved [11]. Various deposition techniques, such as thermal atomic layer deposition (ALD) or plasma-assisted ALD (PA-ALD) [12-15] and plasma-enhanced chemical vapor deposition (PECVD) [16,17] have been employed. A maximum effective surface recombination velocity below 10

cm/s was obtained on low resistivity p-type crystalline silicon substrates by ALD deposition [11,18]. The ALD technique cycles reactant gas insertions and purges in order to achieve a precisely controlled deposition, atomic layer by atomic layer. Therefore, it has been mentioned that typical low deposition rates of ALD limit its application in a commercial production line [19,20]. Other than the deposition methods, plasma oxidation that needs only O_2 and inert gas as plasma gases has attracted much attention as an alternative approach to prepare thin Al_2O_3 films especially for spin tunnel junctions [21-24].

Recently, we have reported high-rate and low-temperature (150 – 400°C) oxidation of Si wafers using stable glow plasma excited at atmospheric pressure (AP) by a 150 MHz very high-frequency (VHF) power [25,26], and demonstrated that AP VHF plasma oxidation at 400°C is capable of producing the SiO_2/Si structure with low D_{it} at the midgap of 1.4×10^{10} $cm^{-2}eV^{-1}$ and moderately high positive Q_f of 5.3×10^{11} cm^{-2} [27]. These properties are desirable for field effect passivation of n-type Si surfaces. On the other hand, for passivation of p-type Si surfaces, low D_{it} and high negative Q_f are required. The objective of the present research is to study the Q_f and D_{it} at AlO_x/Si interface using SiO_2 interlayer prepared by AP VHF plasma oxidation.

5.2 Experimental details

A schematic illustration of an AP plasma oxidation apparatus is shown in Fig.3-1. A parallel-plate electrode with 50 mm diameter was used in this study. The substrates used in the present experiments were n-type (001) oriented CZ-Si wafers (4 inch diameter) with a resistivity of 1 – 10 Ωcm. Si wafers were cleaned by a room temperature chemical cleaning method [28]

and were finished by a diluted HF treatment. The oxidation temperature was controlled at 300 – 400°C by monitoring a thermocouple embedded in the substrate heating stage. For the formation of AlO_x/SiO_2 stacks, SiO_2 films were firstly prepared by O_2/He AP VHF plasma oxidation of Si wafers at 400°C. After depositing an Al metal film on the surface of SiO_2/Si by thermal evaporation, the Al film was oxidized in AP VHF plasma at 400°C. Details of experimental conditions for preparing AlO_x/SiO_2 stacks are summarized in Table 5-1. No post-oxidation anneal was performed for the prepared AlO_x/SiO_2 stacks. In order to investigate Q_f and D_{it}, metal-oxide-semiconductor (MOS) capacitors with 0.5-mm-diameter Al pads were fabricated by vacuum deposition. Ellipsometry (Rudolph Auto EL III) with a wavelength of 632.8 nm was used to determine the thickness of SiO_2 film. The atomic composition was measured by X-ray photoelectron spectroscopy (XPS; ULVAC-PHI Quantum 2000). Transmission electron microscopy (TEM; JEOL JEM-2000FX) observations were performed to determine the thickness of AlO_x film and observe the AlO_x/SiO_2 structure on Si wafer. High-frequency (HF) *C*–*V* measurements were performed on the MOS samples using a 1 MHz C meter/CV plotter (HP 4280A).

Table 5-1 Detailed oxidation conditions for Si and Al .

O_2 concentration (%)	1
He flow rate (slm)	10
Plasma frequency (MHz)	150
Plasma power (W)	1000 – 1500
Plasma gap (mm)	0.8
Substrate temperature (°C)	400
Oxidation time for Si wafer (min)	0.17 – 25
Oxidation time for Al film (min)	5 – 25

5.3 Results and discussion

Figure 5-1 shows experimental plots of the oxide thicknesses for SiO_2 and AlO_x at the mid area between the wafer center and the periphery of the oxide film as a function of oxidation time. SiO_2 films were prepared by AP VHF plasma oxidation of Si wafers for 4 – 25 min at 400°C. For the measurements of Fig.5-1, AlO_x layers were formed by AP VHF plasma oxidation of sufficiently thick Al metal films (~ 50 nm) deposited on the thermally oxidized Si wafer with the SiO_2 thickness of about 100 nm.

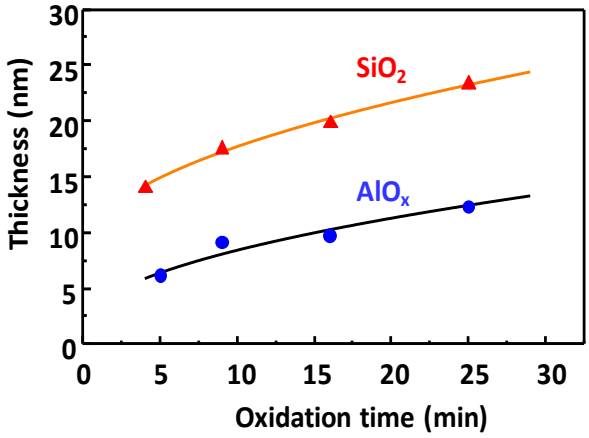

Fig.5-1 Oxide thicknesses for SiO_2 and AlO_x as a function of AP plasma oxidation time at 400°C.

Fig.5-2 shows a cross sectional TEM photograph of AlO_x film grown by the AP plasma oxidation of the thick Al film. The feature of AP plasma oxidation curves for SiO_2 and AlO_x films in Fig.5-1 is that the oxide thickness increases rapidly at the very early stage, and the growth slows down in the later stage. If we assume that the diffusion of oxidizing species (for SiO_2) or metal ions (for AlO_x) through the growing oxide is the rate limiting step, the oxide growth is gradually suppressed as the oxide film becomes thicker. This may indicate that not only SiO_2 but also AlO_x films

grown by AP plasma oxidation for few minutes at 400°C have a continuous and compact structure.

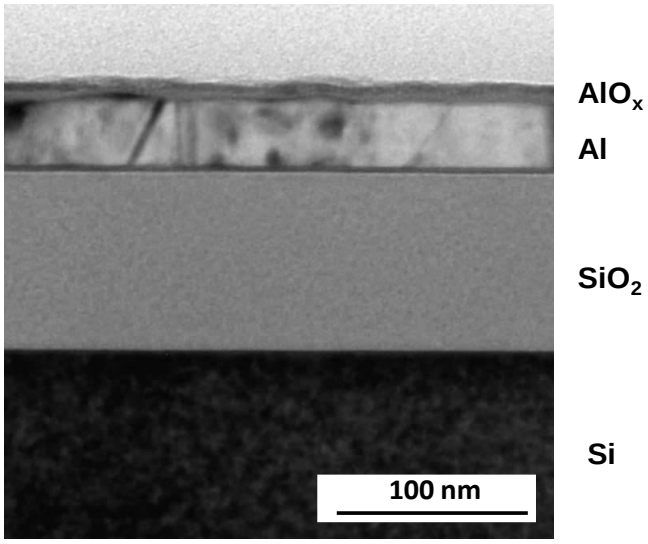

Fig.5-2 Cross-sectional TEM image of the AlO_x film grown by AP VHF plasma oxidation of thick Al film (50 nm) on SiO_2 (100 nm) .

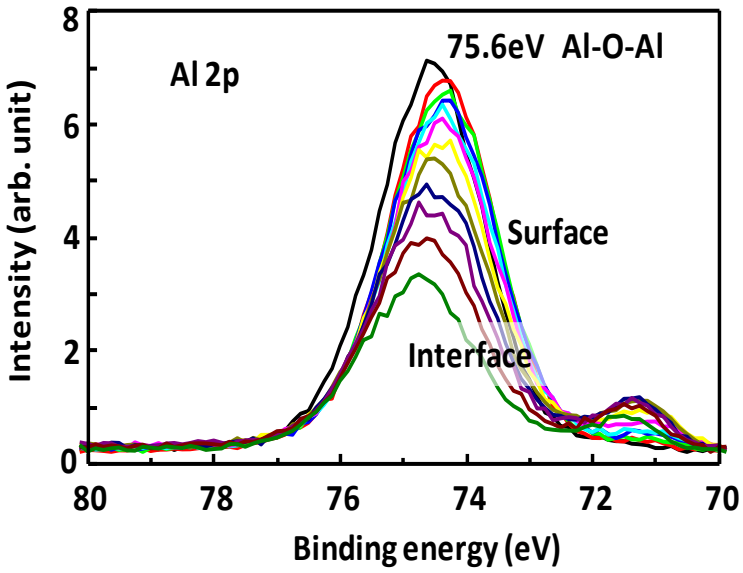

Fig.5-3 XPS spectrum of Al 2*p* from AlO_x film for each sputter etching step. (AP plasma oxidation of Al film at 400°C for 9 min.)

Figure 5-3 shows XPS spectra of Al 2*p* peaks obtained from the AlO_x film in the $AlO_x/SiO_2/Si$ structure formed by AP VHF plasma oxidation of Al film at 400°C for 9 min. In Fig.5-3, the peak energy of 74.7 eV corresponds to the binding energy for $2p_{3/2}$ electrons from Al bound to O in Al_2O_3 [11,29-30]. By increasing the sputter etching steps, the peak intensity decreases and the peak position shows a slight shift to the higher energy side except the one at the surface. Probably, the Al 2*p* spectrum at the surface contains the component associated with the Al-OH bonds at 75.6 eV [11,30], and near the AlO_x/SiO_2 interface it contains the component associated with the Al-O-Si bonds at 76.0 eV [30].

Figure 5-4 shows depth profiles of Al, Si and O concentrations for the AlO_x (8 nm)/SiO_2 (5 nm) stack structure evaluated by XPS as a function of sputter etching time. The ratio of O to Al concentration is approximately 2.0, suggesting an O-rich AlO_x film has been formed in this case. The composition of SiO_2 layer in the stack after the sufficient AP plasma oxidation (9 min) of whole Al layer cannot be determined from Fig.5-4 due to the artifacts of sputter depth profiling. The facts that a stoichiometric SiO_2 is formed by the AP plasma oxidation of Si as reported previously [27] and a clear interface of AlO_x/SiO_2 is observed in the cross-sectional TEM photograph (Fig.5-5) may not agree with the apparent composition variation seen in Fig.5-4.

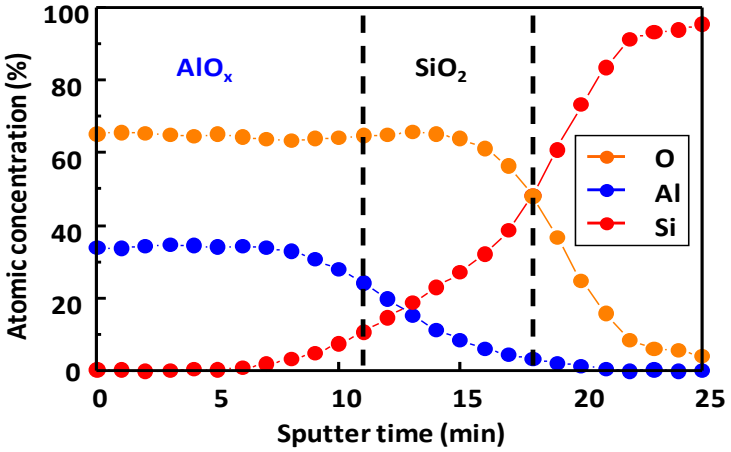

Fig.5-4 XPS depth profiling data for AlO_x (8 nm)/ SiO_2 (5 nm) /Si structure.

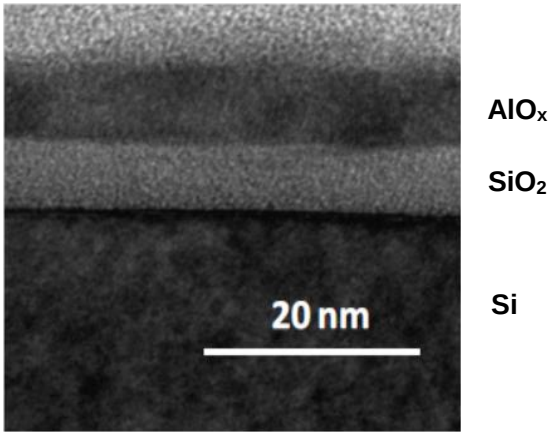

Fig.5-5 Cross-sectional TEM image of $AlO_x/SiO_2/Si$ structure formed by AP plasma oxidation.

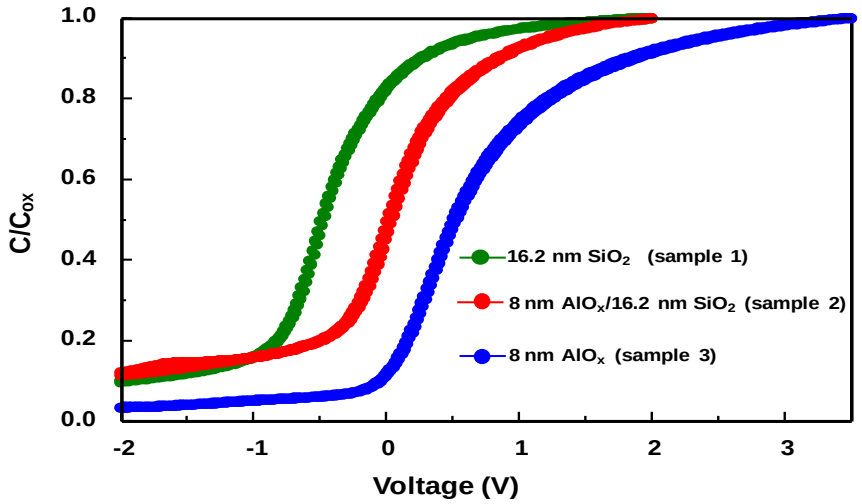

Fig.5-6 Typical HF *C–V* characteristics of three capacitors utilizing SiO_2 monolayer (sample 1), AlO_x/SiO_2 stack (sample 2) and AlO_x monolayer (sample 3) as gate dielectrics, respectively.

In Fig. 5-4, it is deduced that a certain amount of Si diffuses into Al, and Al–O–Si compounds form at the Al/Si front [31,32]. It has been suggested that the solid solubility of Si in Al is higher than that of Al in Si, which enables the diffusion of Si into Al [33,34]. Our result implies that the existence of a SiO_2 interlayer not only plays an important role in improving the sharpness of the interface, but also prevents the direct interaction of Al and Si during AlO_x growth. From the *C–V* measurements, the relative permittivity of the prepared AlO_x film by AP plasma oxidation was approximately 7.9.

Figure 5-6 shows typical HF *C–V* characteristics of three capacitors utilizing SiO_2 monolayer (sample 1), AlO_x/SiO_2 stack (sample 2) and AlO_x monolayer (sample 3) as gate dielectrics. The flatband voltage V_{FB} for each sample is determined by the voltage at which the measured capacitance equals the calculated flatband capacitance C_{FB} [35],

$$C_{\mathrm{FB}} = \frac{C_0 C_{\mathrm{SF}}}{C_0 + C_{\mathrm{SF}}} \qquad (1)$$

where C_0 is the capacitance in accumulation and C_{SF} is the Si surface capacitance at the flat band. C_{SF} is given by

$$C_{\mathrm{SF}} = \frac{K_{\mathrm{Si}} \varepsilon_0}{\lambda_{\mathrm{D}}} \cdot A \qquad (2)$$

where K_{Si} is the relative permittivity of Si, ε_0 is the vacuum permittivity, A is the Al pad area and λ_{D} is the extrinsic Debye length in Si. V_{FB} for the *C–V* curve of sample 1 is negative, indicating that the net charges stored in the film are positive. V_{FB}s for samples 2 and 3 are positive, indicating the charges stored in these samples are negative.

The total charge density (Q_{tot}) in the stack is calculated from

$$Q_{\mathrm{tot}} = \frac{-(V_{\mathrm{FB}} - W_{\mathrm{MS}}) \cdot C_0}{q \cdot A} \qquad (3)$$

with the work function difference (W_{MS}) between Al and n-Si

$$W_{\mathrm{MS}} = -0.6\ \mathrm{eV} + \frac{kT}{q} ln \frac{N_D}{n_i} \qquad (4)$$

where N_{D} is the donor density and n_{i} is the intrinsic carrier density [36]. The value of Q_{tot} have been estimated to be $+6.5 \times 10^{11}$, -0.5×10^{11} and $-6.4 \times 10^{11}\ \mathrm{cm}^{-2}$ for samples 1, 2 and 3, respectively. D_{it} has been estimated by Terman's method to be 3.5×10^{11}, 2.7×10^{11} and $2.7 \times 10^{12}\ \mathrm{cm}^{-2}\mathrm{eV}^{-1}$ for samples 1, 2 and 3, respectively. It is important to mention here that D_{it} is

approximately one order of magnitude higher for monolayer AlO_x (sample 3) than others with SiO_2 interlayers. This may be due to the inter-diffusion of Si and Al for the monolayer AlO_x case, which leads to the deterioration of interface qualities under the AP VHF plasma oxidation. By inserting SiO_2 interlayer between the AlO_x and Si, D_{it} decreases from the order of 10^{12} to 10^{11} $cm^{-2}eV^{-1}$. Since D_{it} is the critical parameter for passivating layers, we suppose that the existence of a SiO_2 interlayer plays an important role in decreasing D_{it} at the interface.

Systematic investigations of D_{it} and Q_{tot} for $AlO_x/SiO_2/Si$ stacks with different SiO_2 thickness were performed by HF *C–V* measurements. The thickness of SiO_2 interlayer obtained by AP plasma oxidation of Si wafer for 0.17, 1, 5, 9, 16 and 25 min is 5.0, 8.0, 13.5, 16.2, 18.3 and 23.5 nm, respectively. As shown in Fig.5-7, HF *C–V* curves shift to a negative gate bias direction with increasing the thickness of SiO_2 interlayer.

The total charge density Q_{tot} is determined by

$$Q_{\mathrm{tot}} = Q_{\mathrm{f}} + Q_{\mathrm{m}} + Q_{\mathrm{ot}} + Q_{\mathrm{it}} \qquad (5)$$

where Q_f is the fixed charge density, Q_m is the density of mobile ionic charges, Q_{ot} is the charge density trapped in the bulk of the oxide and Q_{it} is the charge density trapped at the interface states [35]. Since no significant hysteresis is seen on the *C–V* curves in Fig. 5-7, Q_m may be neglected. Q_{it} depends on the nature (acceptor or donor type), the energy distribution and the occupancy of the interface states. The interface state density near the band edge region is very high, but it can be assumed to have the nature similar to the band states and their contribution to Q_{it} may be neglected. D_{it} near the midgap region is thought to be related with Si dangling bonds at

the interface, and they are of amphoteric nature. Therefore, it is difficult to estimate Q_{it}, unless the detailed nature of the interface states is clear. When the interface state density near the midgap is much lower than Q_f, Q_{it} may be neglected [35]. Concerning Q_{ot} in SiO_2 and Al_2O_3 films, most of the results revealed that oxide charges are located at SiO_2/Si and Al_2O_3/SiO_2 interfaces and Q_{ot} may be neglected [11,35-36].

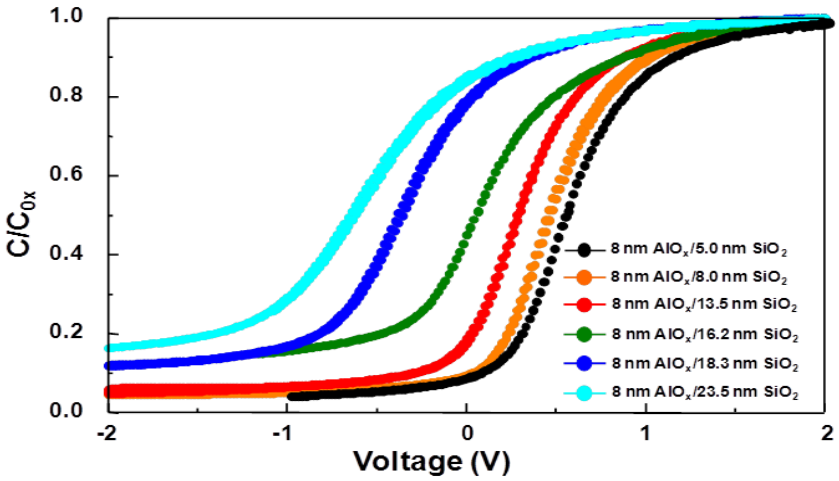

Fig.5-7 HF C–V characteristics of the MOS capacitors using AlO_x/SiO_2 stacks as an insulator. With decreasing SiO_2 interlayer thickness, *C–V* curves shift to a positive gate bias direction.

In the AlO_x/SiO_2/Si stack structure, Q_f is related with the two components, those are positive fixed charges at SiO_2/Si interface and negative fixed charges at AlO_x/SiO_2 interface. It has been suggested that excess Si (trivalent Si) or the loss of an electron from excess O centers (nonbridging O) close to the Si/SiO_2 interface is the origin of positive fixed charges [37]. On the origin of the negative fixed charges in AlO_x, there are several models. According to the literature [36,38], it is considered to be related with tetrahedrally coordinated Al in AlO_4^- units which are present

at the Al_2O_3/SiO_2 interface since the tetrahedral coordination of SiO_2 structure stabilize the excessive amount of AlO_4^- units. Al vacancies and O interstitials have been also proposed as the origin of the negative charges in Al_2O_3 [39]. Recently, it has been shown that the negative charge density in $Al_2O_3/SiO_2/Si$ system exponentially decreases with increasing SiO_2 thickness [40,41]. It is suggested that the charge injection through the SiO_2 film plays a role in forming negative charges at the SiO_2/Al_2O_3 interface [11,40-42] assuming that Al vacancies and O interstitials are the origins of the negative charges [11,41,42].

Table 5-2 shows Q_{tot} and D_{it} for $AlO_x/SiO_2/Si$ structures with different SiO_2 thicknesses (d_S). d_S in the $AlO_x/SiO_2/Si$ structure is determined from C_0 with the assumed AlO_x thickness of 8 nm and the relative permittivity of 7.9. d_S is slightly larger than that in the simple SiO_2/Si structure due to the additional AP plasma oxidation process for Al. The positive fixed charge density (Q_S) for SiO_2/Si in Table 5-2 is the measured value using simple SiO_2/Si structures with different SiO_2 thicknesses after the annealing in N_2, which simulates the following AP plasma oxidation process of Al at 400°C for 9 min. Since Q_S is almost independent of the oxidation time for SiO_2 formation, it can be said that the positive fixed charges in SiO_2 formed by AP plasma oxidation is located at the SiO_2/Si interface similar to the thermally oxidized Si. In Table 5-2, D_{it} values estimated by Terman's method might be unreliable when D_{it} is lower than 10^{11} cm^{-2}. Although a reliable quasi-static *C–V* measurement could not be performed for the $AlO_x/SiO_2/Si$ structure with d_s = 5 nm due to the leakage current, D_{it} is deduced to be lower than 10^{11} $cm^{-2}eV^{-1}$.

Table 5-2 Total charge density (Q_t) and interface state density (D_{it}) for $AlO_x/SiO_2/Si$ structure as a function of AP plasma oxidation time (t_S) for SiO_2 interlayer formation. The thickness of AlO_x layer is 8.0 nm. d_S is the thickness of SiO_2 layer. Q_S is the fixed charge density in the simple SiO_2/Si structure.

t_S	d_S	Q_t	Q_S	D_{it}
min	nm	10^{11} cm^{-2}	10^{11} cm^{-2}	10^{11} cm^{-2}eV^{-1}
0.17	5.0	–11.0	4.2	0.7
1	8.0	–7.4	4.8	0.9
5	13.5	–3.7	3.5	5.5
9	16.2	–3.0	3.6	2.7
16	18.3	+0.6	5.0	1.8
25	23.5	+1.1	4.3	3.3

As shown in Table 5-2, a high Q_{tot} of negative charges in the order of 10^{12} cm^{-2} is obtained for the AlO_x/SiO_2 stack with thin SiO_2 thickness. With increasing d_S, Q_{tot} decreases and switches the polarity from negative to positive. Terlinden *et al*. [41] have reported that effective charge density in ALD or PECVD $Al_2O_3/SiO_2/Si$ structure decreases rapidly for increasing SiO_2 thickness and switches the polarity from negative to positive at the thickness of about 5 nm for n-type Si substrate. This switch in polarity has been explained by tunneling of electrons through the SiO_2 layer into defect states at Al_2O_3/SiO_2 interface as well as the presence of positive fixed charges at the SiO_2/Si interface [11,40-42]. Although, our results in Table 5-2 may be compatible with this explanation, the SiO_2 interlayer thickness (between 9 and 16 nm) at which the polarity of Q_{tot} switches seems to be much larger than 5 nm reported by Terlinden *et al*. [41]. There are several possible explanations for this discrepancy. Firstly, other charging mechanism of defect states at Al_2O_3/SiO_2 interface than electron tunneling such as the ultraviolet light excitation can contribute under the AP plasma

exposure which shows high plasma emission intensity. Secondly, since D_{it} in the stack with thicker d_s is relatively high in the present experiments (Table 5-2), Q_{it} due to the occupied D_{it} of acceptor type cannot be negligible, which contributes to the negative charges in Q_{tot}. Further study is needed to clarify the charging mechanism for AlO_x/SiO_2 stacks prepared by AP plasma oxidation.

5.4 Conclusions

AlO_x films are prepared by AP VHF plasma oxidation of Al metal films on SiO_2/Si at 400°C, and are characterized by XPS, TEM and *C-V* measurements. XPS analysis shows that the prepared AlO_x film is O rich (x ~ 2.0) and the most Al atoms are bound to O in the Al_2O_3 form. The AP VHF plasma oxidation rate is high enough to obtain an AlO_x film thicker than 5 nm with 5 min. Cross sectional TEM observations show that the AlO_x film is continuous and compact with a clear interface is formed between AlO_x and SiO_2. Systematic *C-V* measurements show that thin interfacial SiO_2 layer (5 nm) between AlO_x and Si plays important roles in decreasing interface state density D_{it} from 10^{12} to 10^{11} $cm^{-2}eV^{-1}$ and in forming a high negative charge density in the order of 10^{12} cm^{-2}. With increasing the SiO_2 interlayer thickness, the total negative charge density in the AlO_x/SiO_2/Si stack decreases and switches to positive with higher SiO_2 thickness than about 10 nm. From the view point of Si surface passivation, since the negative charge density is high in the order of 10^{12} cm^{-2} and the interface state density is moderately low in the order of 10^{11} $cm^{-2}eV^{-1}$, the AlO_x/SiO_2 structure prepared by AP VHF plasma oxidation has a potential for field-effect passivation of p-type Si surfaces.

References

[1] K. Wefers and C. Misra, ALCOA Technical Report No. **19** (1987).

[2] I. Levin and D. Brandon, J. Am. Ceram. Soc. **81** (1998) 1955.

[3] R. S. Zhou and R. L. Snyder, Acta Crystallogr. B **47** (1991) 617.

[4] J. Robertson, Eur. Phys. J. Appl. Phys. **28** (2004) 265.

[5] T. Murayama and T. Nakai, Appl. Phys. Lett. **58** (1991) 2079.

[6] D. Yan, J. He, X. Li, L. Jianxin and Z. H. Ding, Surf. Coat. Technol. **141** (2001) 1.

[7] R. K. Nahar and V. K. Khanna, Sens. Actuators Int. J. Electron. **52** (1982) 557.

[8] B. Hoex, J. J. Gielis, M. C. M. van de Sanden and W. M. M. Kessels, J. Appl. Phys. **104** (2008) 113703.

[9] K. Kimoto, Y. Matsui, T. Nabatame, T. Yasuda, T. Mizoguichi, I. Tanaka and A. Toriumi, Appl. Phys. Lett. **83** (2003) 4306.

[10] M. J. Kerr and A. Cuevas, Semicond. Sci. Technol. **17** (2002) 35.

[11] G. Dingemans and W. M. M. Kessels, J. Vac. Sci. Technol. A **30** (2012) 040802.

[12] G. Agostinelli, A. Delabie, P. Vitanov, Z. Alexieva, H. F. W. Dekkers, S. De Wolf and G. Beaucarne, Sol. Energy Mater. Sol. Cells **90** (2006) 3438.

[13] B. Hoex, J. Schmidt, P. Pohl, M. C. M. van de Sanden and W. M. M. Kessels, J. Appl. Phys. **104** (2008) 044903.

[14] J. Schmidt, B. Veith and R. Brendel, Phys. Stat. Sol. **3** (2009) 287.

[15] G. Dingemans, R. Seguin, P. Engelhart, M. C. M. van de Sanden and W. M. M. Kessels, Phys. Stat. Sol. **4** (2010) 10.

[16] P. Saint-Cast, D. Kania, M. Hofmann, J. Benick, J. Rentsch and R. Preu, Appl. Phys. Lett. **95** (2009) 151502.

[17] S. Miyajima, J. Irikawa, A. Yamada and M. Konagai, Appl. Phys. Express **3** (2010) 012301.

[18] B. Hoex, S. B. S. Heil, E. Langereis, M. C. M. van de Sanden and W. M. M. Kessels, Appl. Phys. Lett. **89** (2006) 042112.

[19] T. T. Li and A. Cuevas, Phys. Stat. Sol. **3** (2009) 160.

[20] P. Saint-Cast, D. Kania, M. Hofmann, J. Benick, J. Rentsch and R. Preu, Appl. Phys. Lett. **95** (2009) 151502.

[21] C. Deng, M. Otto and A. Lupascu, Appl. Phys. Lett. **104** (2014) 043506.

[22] A. E. T. Kuiper, M. F. Gillies, V. Kottler, G. W. ‘t Hooft, J. G. M. van Berkum, C. van der Marel, Y. Tamminga and J. H. M. Snijders, J. Appl. Phys. **89** (2001) 1965.

[23] A. Quade, H. Wulff, H. Steffen, T. M. Tun and R. Hippler, Thin Solid Films **377-378** (2000) 626.

[24] F. –H. Lu, H. –D. Tsai and Y. –C. Chieh, Thin Solid Films **516** (2008) 1871.

[25] H. Kakiuchi, H. Ohmi, M. Harada, H. Watanabe and K. Yasutake, Appl. Phys. Lett. **90** (2007) 091909.

[26] H. Kakiuchi, H. Ohmi, M. Harada, H. Watanabe and K. Yasutake, Appl. Phys. Lett. **90** (2007) 151904.

[27] Z. Zhuo, Y. Sannomiya, K. Goto, T. Yamada, H. Ohmi, H. Kakiuchi and K. Yasutake, Current Appl. Phys. **12** (2012) S57.

[28] T. Ohmi, J. Electrochem. Soc. **143** (1996) 2957.

[29] T. Gougousi, D. Barua, E. D. Young and G. N. Parsons, Chem. Mater. **17** (2005) 5093.

[30] N. Komatsu, K. Masumoto, H. Aoki, C. Kimura and T. Sugino, Appl. Surf. Sci. **256** (2010) 1803.

[31] R. Rosenberg, M. J. Sullivan and J. R. Howard, in *Thin films– Interdiffusion and Reaction*, J. M. Poate, K. N. Tu and J. W. Mayer, eds. (Wiley, New York, 1978).

[32] T. J. Faith and C. P. Wu, Appl. Phys. Lett. **45** (1984) 470.

[33] J. O. McCaldin and H. Sankur, Appl. Phys. Lett. **19** (1971) 524.

[34] C. S. Pai, E. Cabreros, S. S. Lau, T. E. Seidel and I. Suni, Appl. Phys. Lett. **47** (1985) 652.

[35] D. K. Schroder, *Semiconductor Material and Device Characterization*, 2nd ed. (Wiley, New York, 1998).

[36] R. S. Johnson, G. Lucovsky and I. Baumvol, J. Vac. Sci. Technol. A **19** (2001) 1353.

[37] S. M. Sze, *Physics of Semiconductor Devices*, 2nd ed. (Wiley, New York, 1981) p. 390.

[38] K. Kimoto, Y. Matsui, T. Nabatame, T. Yasuda, T. Mizoguchi, I. Tanaka and A. Toriumi, Appl. Phys. Lett. **83** (2003) 4306.

[39] K. Matunaga, T. Tanaka, T. Yamamoto and Y. Ikuhara, Phys. Rev. B **68** (2003)

085110.

[40] S. Mack, A. Wolf, C. Brosinsky, S. Schmeisser, A. Kimmerle, P. S-. Cast, M. Hofmann and D. Biro, IEEE, J. Photovoltaics **1** (2011) 135.

[41] N. M. Terlinden, G. Dingemans, V. Vandalon, R. H. E. C. Bosch and W. M. M. Kessels, J. Appl. Phys. **115** (2014) 033708.

[42] G. Dingemans, N. M. Terlinden, M. A. Verheijen, M. C. M. van de Sanden and W. M. M. Kessels, J. Appl. Phys. **110** (2011) 093715.

Chapter 6

Summary

The PV market is still dominated by crystalline silicon (c-Si) solar cells, especially due to the wide abundance of Si and its non-toxicity. On the other hand, in order to reduce the cost of c-Si solar cells, the developmental trend of Si photovoltaics moves toward much thinner cells than 150 μm. However, the energy conversion efficiencies of thin c-Si solar cells are strongly limited by the surface recombination of photo-generated carriers. Therefore, surface passivation is a key requirement for optimizing the performance of thin c-S solar cells. The purpose of this study is to develop a new and highly efficient film formation technology that makes it possible to fabricate passivation films (SiO_2, SiO_xN_y and AlO_x) at low temperatures ($T \leq 400°C$) using a stable glow plasma excited at atmospheric pressure (AP) by a 150 MHz very high-frequency (VHF) power. The important results of the present study are summarized as follows.

Following Chapter 1 (Introduction) and Chapter 2 which reviews the present status of plasma oxidation technology, Chapter 3 describes the results of high-rate and low-temperature (300–400°C) oxidation of Si wafers to prepare SiO_2 passivation films using a stable glow 0.5–5% O_2/He plasma excited at atmospheric pressure by a 150 MHz VHF power. From the characterization results of ellipsometry, X-ray photoelectron spectroscopy, Fourier transmission infrared spectroscopy and transmission electron microscopy, it can be said that the AP plasma oxidation is capable of producing high-quality SiO_2 films comparable to those of high-temperature thermal oxides. The oxidation rates for AP plasma

oxidation of Si wafers at 400°C are faster than those by thermal dry oxidation at 900°C. Moreover, the high quality SiO_2 film with low interface state density (D_{it}) of 1.4×10^{10} $cm^{-2}eV^{-1}$ and moderately high fixed charge density (Q_f) of 5.3×10^{11} cm^{-2} is achieved by optimizing the formation conditions. The estimated effective surface recombination velocity (S_{eff}) based on the Schockley-Read-Hall recombination model was below 10 cm/s, which is low enough to realize high-efficiency Si solar cells. Therefore, it can be said that SiO_2 films prepared by the AP plasma oxidation are promising for surface passivation of Si wafers.

Chapter 4 describes the formation of SiO_xN_y films with a low nitrogen concentration (< 4 %) prepared on Si substrates at 400°C by AP plasma oxidation-nitridation process using O_2 and N_2 diluted in He. Interface properties of SiO_xN_y films have been investigated by analyzing high-frequency and quasistatic capacitance-voltage (C-V) characteristics of metaloxide-semiconductor capacitors. It is found that addition of N into the oxide increases both D_{it} and positive Q_f. After forming gas anneal, D_{it} decreases largely with decreasing N_2/O_2 flow ratio from 1 to 0.01 while the change of Q_f is insignificant. These results suggest that low N_2/O_2 flow ratio is a key parameter to achieve a low D_{it} and relatively high Q_f, which is effective for field effect passivation of n-type Si surfaces.

In Chapter 5, formation and characterization of AlO_x films on c-Si wafers by AP VHF plasma oxidation at 400°C is introduced. Systematic C-V measurements showed that an interfacial SiO_2 layer between AlO_x and Si plays important roles in decreasing the D_{it} from 10^{12} to 10^{11} $cm^{-2}eV^{-1}$ and forming a negative fixed charge density in AlO_x higher than 10^{12} cm^{-2}. By decreasing the SiO_2 interlayer thickness from about 20 to 5 nm, the polarity of overall fixed charges changes from positive ($Q_f = 10^{11}$ cm^{-2}) to

negative (10^{12} cm^{-2}).

Chapter 6 describes the summary of the results. In conclusion, SiO_2, SiO_xN_y and AlO_x films prepared by AP VHF plasma oxidation at 400°C is useful for effective field-effect passivation of Si surfaces. The AP VHF plasma oxidation method has several advantages such as the increase in oxidation rates, the reduction of the processing temperature and the absence of harmful chemical residue. Moreover, since the open-air AP plasma oxidation process is principally possible to realize, it is expected to be useful for many industries as a high-throughput process for preparing functional oxide films.

Publications

1. Z. Zhuo, Y. Sannomiya, K. Goto, T. Yamada, H. Ohmi, H. Kakiuchi and K. Yasutake, Formation of SiO_2/Si structure with low interface state density by atmospheric-pressure VHF plasma oxidation. ***Current Applied Physics* 12** (2012) S57-S62.

2. Z. Zhuo, Y. Sannomiya, Y. Kanetani, T. Yamada, H. Ohmi, H. Kakiuchi and K. Yasutake, Interface properties of SiO_xN_y layer on Si prepared by atmospheric-pressure plasma oxidation-nitridation. ***Nanoscale Research Letters* 8** (2013) 201.

3. Z. Zhuo, Y. Fujiwara, T. Yamada, H. Ohmi, H. Kakiuchi and K. Yasutake, Characterization of AlO_x thin films prepared by AP VHF plasma oxidation. ***to be submitted.***

Conferences

1. Poster

1) Z. Zhuo, T. Ohnishi, K. Goto, H. Ohmi, H. Kakiuchi and K. Yasutake Atmospheric-Pressure Plasma Oxidation Process for Passivation of Si Surface.
精密工学会2010年度関西地方定期学術講演会（2010年5月28日，京都大学）

2) 後藤一磨，卓澤騰，大西崇之，三宮佑太，大参宏昌，垣内弘章，安武潔
大気圧プラズマ酸化による太陽電池用Si表面パッシベーション膜の形成
精密工学会 2010年度 秋季大会学術講演会（2010年9月27-29日， 名古屋大学）

3) Z. Zhuo, T. Ohnishi, K. Goto, Y. Sannomiya, H. Ohmi, H. Kakiuchi and K. Yasutake Atmospheric-Pressure Plasma Oxidation Process for Passivation of Si Surface.
Conf. Proc. 7th ICRP and 63rd GEC, (Oct. 4-8, 2010, Paris) CTP-090.

4) 卓澤騰，大西崇之，後藤一磨，三宮佑太，大参宏昌，垣内弘章，安武潔
Surface Passivation of N-type Si Surfaces Using SiO_2 Grown by Atmospheric-Pressure Plasma Oxidation.
2011年度 精密工学会春季大会学術講演会（2011年3月14-16日，東洋大学）

5) 三宮佑太，後藤一磨，卓澤騰，金谷優樹，山田高寛，大参宏昌，垣内弘章，安武潔
大気圧プラズマを用いたシリコン表面パッシベーションプロセスの開発
精密工学会 2011年度関西地方定期学術講演会（2011年6月30日，兵庫県立大学）

6) 後藤一磨，卓澤騰，三宮佑太，金谷優樹，山田高寛，大参宏昌，垣内弘章，安武潔.
大気圧プラズマ酸化による太陽電池用Si表面パッシベーション技術の開発
2011年度 精密工学会秋季大会学術講演会（2011年9月20-22日，金沢大学）

7) Y. Sannnomiya, K. Goto, Z. Zhuo, Y. Kanetani, T. Yamada, H. Ohmi, H. Kakiuchi and K. Yasutake
Atmospheric-Pressure Plasma Oxidation Process for Si Surface Passivation.
Abst. 15th International Conference on Thin Films, 2011 (Nov. 8-11, 2011, Kyoto, Japan)

8) 卓澤騰，三宮佑太，後藤一磨，山田高寛，大参宏昌，垣内弘章，安武潔
Surface passivation of Si by atmospheric-pressure plasma oxidation at low temperatures
2012年度 精密工学会春季大会学術講演会（2012年3月14-16日，首都大学東京）

9) 三宮佑太，後藤一磨，卓澤騰，金谷優樹，山田高寛，大参宏昌，垣内弘章，安武潔
大気圧VHFプラズマによるシリコン表面パッシベーションプロセスの開発
2012年春季 第59回応用物理学関係連合講演会（2012年3月15-18日，早稲田大学）

10) Z. Zhuo, Y. Sannnomiya, T. Yamada, H. Ohmi, H. Kakiuchi andK. Yasutake
Atmospheric-Pressure VHF Plasma Oxidation Process for Passivation of Si Surface.
精密工学会2012年度関西地方定期学術講演会（2012年6月15日，立命館大学）

11) 三宮佑太，金谷優樹，卓澤騰，山田高寛，大参宏昌，垣内弘章，安武潔
大気圧プラズマ酸化によるSiO_2の低温形成
2012年秋季 第73回応用物理学会学術講演会（2012年9月11-14日，愛媛大学・松山大学）

2. Oral

1) Z. Zhuo, T. Ohnishi, K. Goto, Y. Sannomiya, H. Ohmi, H. Kakiuchi and K. Yasutake
Development of Atmospheric-Pressure Plasma Oxidation Process for Surface Passivation of Si.
Ext. Abst. 3rd Int. Symp. on Atomically Controlled Fabrication Technology (Nov. 24-26, 2010, Osaka)

2) Z. Zhuo, K. Goto, Y. Sannomiya, Y. Kanetani, T. Yamada, H. Ohmi, H. Kakiuchi and K. Yasutake
Formation of SiOxNy Films for Passivation of Si Surfaces by Atmospheric-Pressure Plasma Oxidation.
Ext. Abst. 4th Int. Symp. on Atomically Controlled Fabrication Technology (Oct. 31-Nov. 2, 2011, Osaka)

3) Z. Zhuo, Y. Sannomiya, Y. Kanetani, Y. Fujiwara, T. Yamada, H. Ohmi, H. Kakiuchi, and K. Yasutake
Formation of Passivation Films for Si Surfaces by Atmospheric-Pressure VHF Plasma Oxidation.
Ext. Abst. 5th International Symposium on Atomically Controlled Fabrication Technology (Oct. 22-24, 2012, Osaka, Japan)

Acknowledgements

This thesis could not be achieved without the help and support of many people who are gratefully acknowledged here. At the very first, I'm honored to express my deepest gratitude to my dedicated supervisor, Prof. Kiyoshi Yasutake, with whose able guidance I could have worked out this thesis. He has offered me valuable ideas, suggestions and criticisms with his profound knowledge and rich research experience. His patience and kindness are greatly appreciated. Besides, he always puts high priority on my dissertation writing and is willing to discuss with me anytime he is available. I'm very much obliged to his efforts of helping me complete the dissertation.

I'm extremely grateful to Prof. Kazuto Yamauchi, Prof. Heiji Watanabe and Prof. Hiroaki Kakiuchi, whose meticulous guidance and invaluable suggestions are indispensable to the completion of this thesis.

I also thank Prof. Hiromasa Ohmi and Prof. Takahiro Yamada much for their time and guidance. I wish to extend my thanks to Mr. Akihiro Takeuchi, for his technical assistance of the study.

Thanks are also given to labmates, who never failed to give me great encouragement and suggestions. Special thanks should go to Mr. Yuta Sannomiya his kind help in instrument operation and sample characterization. I am thankful to all my friends for their thoughtfulness and encouragement.

"Global COE program" and "Japanese government" are also gratefully acknowledged for their financial supports.